Ocean Engineering 266 (2022) 112749

Contents lists available at ScienceDirect

Ocean Engineering

journal homepage: www.elsevier.com/locate/oceaneng

A meta-model for added resistance in waves

Young-Rong Kim *, Ehsan Esmailian, Sverre Steen

Department of Marine Technology, Norwegian University of Science and Technology (NTNU), Trondheim, 7052, Norway

ARTICLE INFO

Keywords:
Semi-empirical method
Added wave resistance
Propulsion power
Arbitrary wave heading

ABSTRACT

In this paper, we perform a comprehensive study of various semi-empirical methods using publicly accessible experimental data on added resistance in waves with different ship types and conditions. Based on the analysis results, a new method (So-called "Combined method") is proposed, combining two existing methods, which are available in arbitrary wave headings. The results from the two methods are combined smoothly using a tangent hyperbolic function according to wavelengths and wave headings. The coefficients constituting the function are tuned to minimize mean squared error between predictions and model experiments. Finally, the new Combined method is verified by full-scale measurements of a general cargo ship and a container ship, and it seems to give good agreement with measurements in all analysis areas, compared to existing semi-empirical methods. Especially, it showed better performance in estimating added wave resistance at high waves, resonance frequencies, arbitrary waves, and low speeds.

1. Introduction

An operating ship experiences additional resistance due to the surrounding weather conditions, resulting in speed reduction and increased fuel consumption, which can be directly related to greenhouse gas emissions. Traditionally, this fact has been of great interest to ship designers and operators from the perspective of speed/power performance. Moreover, with the increasing interest in atmospheric environmental issues recently, IMO has set the EEDI to limit greenhouse gas emissions. In this regard, it is even more necessary to estimate the added resistance of a ship in an accurate and efficient way for the initial design and the management of operations of a ship.

Many theoretical methods have been developed for calculating the added resistance of ships. Havelock (1942) proposed a method of calculating added resistance by integrating longitudinal pressure on the wetted surface of a ship, and Boese (1970) developed a near-field direct pressure integration method using strip theory. Maruo (1957) first introduced the far-field method based on momentum conservation, and it was expanded in later studies (Joosen, 1966; Maruo, 1960, 1963). Radiated energy approach based on Maruo's far-field method was introduced by Gerritsma and Beukelman (1972), and Salvesen (1978) achieved satisfactory results by applying it to the motion of the ship obtained from the strip theory. Faltinsen (1980) presented an asymptotic formula, assuming the added resistance of wall-sided hull forms in short waves.

Panel methods based on potential theory for computing added wave resistance has been extensively studied by many authors (Joncquez, 2009; Kim and Kim, 2011; Seo et al., 2013; Söding et al., 2014; Lee et al., 2021). However, since most approaches were limited to linear theory, it was generally difficult to accurately calculate the non-linear effect. There were also non-linear panel methods, but they had problems with stability and robustness, and long computational time. Meanwhile, along with the improvement of computational power, Computational Fluid Dynamics (CFD) method based on Reynolds-Averaged Navier–Stokes (RANS) has been widely applied (Orihara and Miyata, 2003; Guo et al., 2012; Sadat-Hosseini et al., 2013; Simonsen et al., 2014; Sigmund and El Moctar, 2018; Lee et al., 2021; T. Kim et al., 2021). It had the advantage of being able to consider nonlinear effects and showed good results overall. However, the output results from the 3D panel method and the RANS equations solver vary depending on the calculation grid and large computational time is required, which leads to a struggle in terms of practicability (Shigunov et al., 2018). Another problem is that they require detailed hull shapes to predict added resistance, which in some cases could serve as an important constraint.

Alternatively, simplified methods based on theory and experimental results have been developed, which could easily estimate added resistance with only a few ship parameters compared to the methods covered earlier. The semi-empirical formula for the added resistance due to wave reflection was first proposed by Fujii (1975), and later further tuned based on more experimental data by Takahashi (1988) and Tsujimoto et al. (2008). In parallel with these studies, for the ship motion-induced added resistance, Jinkine and Ferdinande (1974)

* Corresponding author.
E-mail address: youngrong.kim@ntnu.no (Y. Kim).

https://doi.org/10.1016/j.oceaneng.2022.112749
Received 27 October 2021; Received in revised form 24 September 2022; Accepted 26 September 2022

Nomenclature

Abbreviations

CFD	Computational Fluid Dynamics
COG	Course Over Ground
ECMWF	European Centre for Medium-Range Weather Forecasts
EEDI	Energy Efficiency Design Index
GPS	Global Positioning System
IMO	International Maritime Organization
ITTC	International Towing Tank Conference
M/E	Main engine
MAE	Mean Absolute Error
MSE	Mean Squared Error
RANS	Reynolds-Averaged Navier–Stokes
RMSE	Root Mean Squared Error
STA-JIP	Sea Trial Analysis Joint Industry Project

Nomenclature

α	Wave heading. The wave angle relative to the ship's heading (180 degrees: head waves)
ΔC_F	Roughness allowance
η_T	Overall efficiency
Γ	Gamma function
$\hat{C}_{aw}$	Estimated non-dimensional added wave resistance coefficient
λ	Wave length
ω	Circular wave frequency
ρ	Water density
θ	Primary wave direction
ζ_a	Wave amplitude
a	Slope adjustment Coefficient of a tangent hyperbolic function (Wave frequency)
a_2	Speed correction factor used in wave motion-induced added resistance
B	Breadth
b	Center position adjustment Coefficient of a tangent hyperbolic function (Wave frequency)
c	Slope adjustment Coefficient of a tangent hyperbolic function (Wave heading)
C_B	Block coefficient
C_{aw}	Non-dimensional added wave resistance coefficient
C_{H_s}	Wave height correction factor
$C_{T,Data}$	Total resistance coefficient in calm condition obtained from in-service data
$C_{T,Emp}$	Total resistance coefficient in calm condition estimated from empirical methods
C_T	Total resistance coefficient
d	Center position adjustment Coefficient of a tangent hyperbolic function (Wave heading)
E	Directional wave spectrum
F_n	Froude's number
G	Angular distribution function
g	Gravity acceleration
H_s	Significant wave height
k_{yy}	Pitch gyration
L	Length between perpendiculars
L_E	Length of entrance
L_R	Length of run
P_B	Engine brake power
P_{EST}	Ship propulsion power estimated from the empirical method
P_{MEAS}	Ship propulsion power measured on-board
R	Pearson's correlation coefficient
R_{aw}	Added resistance in regular waves
R_{beam}	Added wave resistance in beam waves
R_{calm}	Calm water resistance
$R_{following}$	Added wave resistance in following waves
R_{head}	Added wave resistance in head waves
R_{total}	Total resistance
R_{wave}	Mean wave resistance increase in irregular waves
R_{wind}	Added resistance due to wind
S	Standard wave frequency spectrum
S_w	Wetted surface area
T	Mean draft
T_m	Mean wave period
V	Ship's speed
V_d	Ship's design speed

developed a formula that simplifies the resistance in long waves based on the experimental data of fast cargo ships. Two simple methods have been developed by STA-JIP to correct the added resistance in waves for sea trial conditions (Boom et al., 2013). The STAWAVE-1 method assumes that the wave reflection contribution dominates the added resistance. From this approach, a practical equation that simplifies the reflection-induced added resistance in irregular waves by approximating the waterline geometry on the bow section and the beam of the ship was presented. Contrary to this, STAWAVE-2 method considers both reflection and radiation contribution in estimating the transfer function for the added wave resistance. Liu and Papanikolaou (2016) originally proposed a statistical method of combining Faltinsen (1980) and Jinkine and Ferdinande (1974). In subsequent studies (Liu and Papanikolaou, 2019, 2020), they introduced wave heading-based trigonometric functions to their previous equation and expanded it to enable calculation for small draft, ballast conditions, and arbitrary waves by regression analysis based on extensive experimental data. Lang and Mao (2020) proposed an added wave resistance model for head seas based on Tsujimoto et al. (2008) and Jinkine and Ferdinande (1974). It was influenced by the formulas presented in Liu and Papanikolaou's paper (Liu and Papanikolaou, 2016; IMO, 2016), and some of its calculations were modified using their experimental datasets. The proposed method was further updated to allow the calculation of the peak position in arbitrary waves by introducing an encountered frequency correction factor (Lang and Mao, 2021). There are also some simple equations that can directly calculate the added resistance in irregular waves such as Kreitner's method (Kreitner, 1939; ITTC, 2005) and Shopera (Papanikolaou et al., 2015). Most simplified methods have been developed to estimate the resistance of a ship operating in head seas. Although studies for added resistance in arbitrary wave headings have been continuously conducted in recent years, comparative analysis and insight into these methods are still insufficient.

To this regard, we perform a comprehensive study of various semi-empirical methods using publicly accessible experimental data on

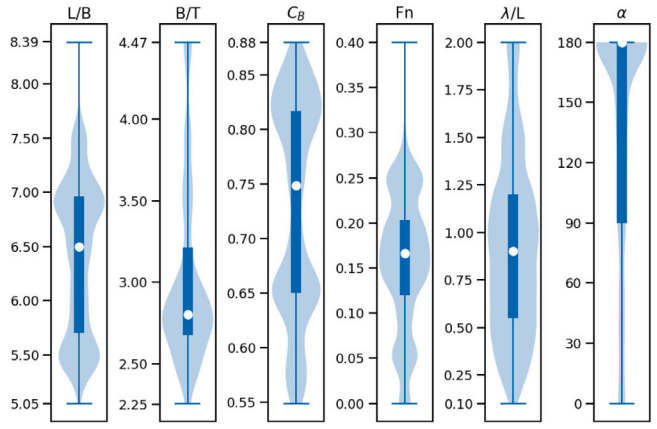

Fig. 1. The composition of the experimental database according to various ship parameters.

added resistance in waves with different ship types and conditions, which is presented in Section 2. Thereafter, in Section 3, a new method is proposed combining two methods available in arbitrary wave headings from the studies of Lang and Mao (2021) and Liu and Papanikolaou (2020), which has been elaborately verified in previous research. The results from these two methods are smoothly connected to wave conditions and wave heading through a combining function. This method is developed for the calculation of added resistance for large fleets of ships, so that robustness, computational efficiency, and applicability to a range of different ship types are priorities. The coefficients of this function are tuned using extensive model test data, and their values are presented according to the ship type. Section 4 verifies the performance of the corresponding method using full-scale measurements of two different ships. Conclusions of the study are addressed in Section 5.

2. Comparison of semi-empirical methods with experimental data

2.1. Description of the experimental data

The results of various publicly accessible experimental data were obtained to consider the general applicability of added resistance in waves to the fleet level, and the performances of the existing semi-empirical models were compared and analyzed. Fig. 1 shows the distribution of main dimensionless parameters of the ships and experimental conditions used in the study. The whisker in the figure indicates the maximum and the minimum range. The box plot shows 25% and 75% quantiles and the circular marker in it represents the median. The data set consists of a total of 2559 samples of approximately 49 ships and 255 different experimental cases. Most of the experiments were conducted at design loading conditions, without trim. More detailed information on the data set is shown in Tables A.1–A.6 in Appendix A.

2.2. Parameter estimation for L_E and L_R

Liu and Papanikolaou (2016) introduced the length of entrance (L_E) parameter in Faltinsen's asymptotic approach to reflect the hull form influence on the component of added resistance due to diffraction effect. Thereafter, corresponding parameters were used in Liu and Papanikolaou (2019, 2020), and Lang and Mao (2020, 2021). L_E is defined as the horizontal distance from the point where the length of the waterline surface reaches 99% of the breadth to Forepeak (Conversely, Length of run (L_R) is the horizontal distance from the point where the length of the waterline surface reaches 99% of the breadth to the endpoint of the waterline), as shown in Fig. 2. These are necessary factors for calculating the entrance angle used in the wave reflection

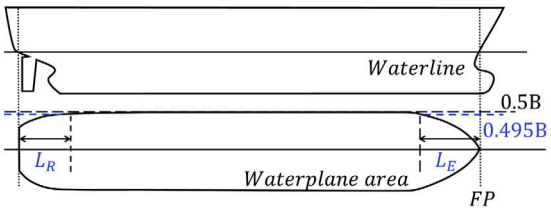

Fig. 2. Definition of length of entrance and run.

contribution to the added resistance. However, L_E and L_R cannot be accurately estimated without detailed hull shape information of the ship. Some authors (Liu et al., 2016; Lang and Mao, 2020, 2021) also listed such values of several ships in their papers.

Fig. 3 shows L_E and L_R according to the length (L_{pp}) of the ships under the design loading conditions we have secured. Overall, L_E and L_R increase in proportion to L_{pp}. L_E decreases as block coefficient (C_B) increases, but in the case of L_R, the trend according to the C_B is not clear. In Fig. 4, dimensionless L_E (L_E/L_{pp}) and dimensionless L_R (L_R/L_{pp}) are plotted as a functions of Block coefficient (C_B), and a linear regression line for each ship type is also plotted. As C_B increases, the dimensionless L_E decreases, and there was a slight difference in the slope and intercept values of the regression line depending on the ship type. On the other hand, the dimensionless L_R according to C_B shows a clear difference in trend according to ship type. The dimensionless L_R values of the tanker, liquefied gas carrier, bulk carrier, and general cargo ship, with relatively high values of C_B, tend to decrease as C_B increases, whereas for relatively slender hull types such as ro-ro/ferry and container ship dimensionless L_R values rather increase. This interpretation is roughly in accordance with what could be expected from knowledge of ship design principles.

Tables 1–2 show the regression equations of dimensionless L_E and L_R for each ship type estimated from Fig. 4. If the detailed hull shape or the L_E and L_R values of the ship were obtainable from the public source, they were used. Otherwise, L_E and L_R values were estimated using the proposed regression equations. It is important to note that one should be careful using regression equations as an alternative to estimating L_E and L_R of the ship, in case the input parameters are outside the range listed in Tables 1–2 or if the ship has a specific hull shape such as a bulbous bow or transom stern. In such cases, there may be gaps between the actual value and the estimated value.

2.3. Comparison of semi-empirical methods in regular waves

In this section, a comparative analysis of several semi-empirical methods for added resistance in regular waves is presented, where the methods from Boom et al. (2013), Lang and Mao (2021), and Liu and Papanikolaou (2020) are denoted as "STA2", "CTH", and "L&P", respectively. STA2 is also compared as a representation of the method that uses only simple ship dimensions although it is applicable only to head waves. Practically, the greater added wave resistance experienced by ships is of main interest. However, when evaluating the degree of error of the model as a residual, the greater the added resistance of the ship, the greater the residual between the predicted value and the experimental value. Therefore, mean squared error (MSE) as defined in Eq. (1), which can give more weight to a larger error by squaring the residual, is used as an evaluation metric. Here, the measurements from model experiments and estimations for the added wave resistance coefficient are compared. As can be found from the figures in the appendices (Fig. B2(a), Fig. B3(c)), there are differences among experimental results for the same ship in the same wave condition, which may be due to the experiment being carried out in different water tank environments. However, the influence of some experimental samples with relative deviations was mitigated by using as many samples as possible.

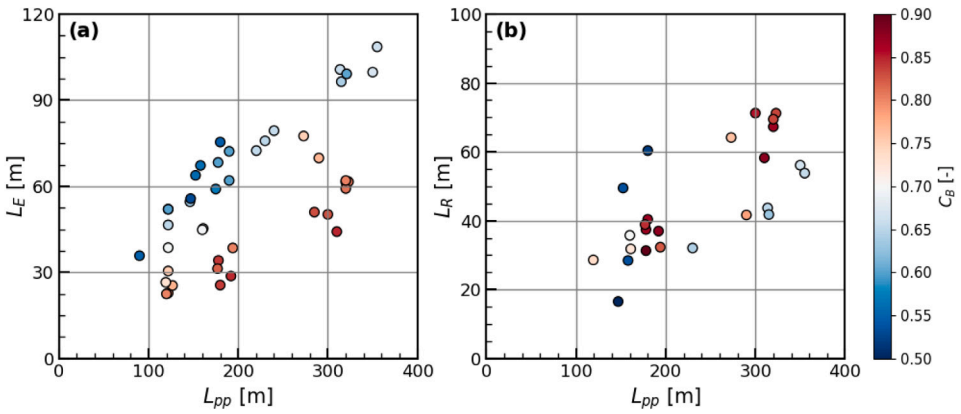

Fig. 3. Scatter plots of (a) length of entrance and (b) length of run against ship length with the color bar showing the block coefficient. (For interpretation of the references to color in this figure legend, the reader is referred to the web version of this article.)

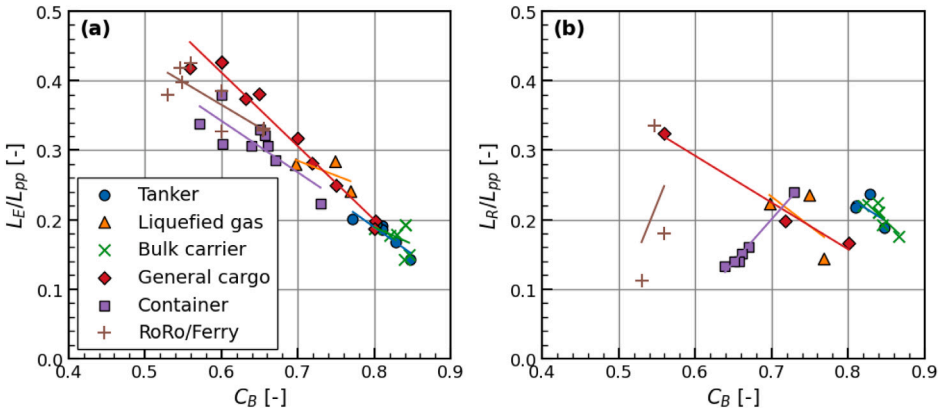

Fig. 4. Scatter plots of dimensionless (a) length of entrance and (b) length of entrance against block coefficient according to the ship type.

Table 1
Regression equations for the dimensionless L_E according to the ship type. x and y in equation represent C_B and L_E/L_{pp}.

Ship type	Range (C_B)	Linear regression equation ($y = ax + b$)	Correlation coefficient (r)
Tanker	0.772–0.847	$y = -0.7833x + 0.8158$	−0.918
Liquefied gas	0.6973–0.7688	$y = -0.4258x + 0.5828$	−0.658
Bulk carrier	0.8–0.8455	$y = -0.4904x + 0.5814$	−0.384
General cargo	0.559–0.801	$y = -1.061x + 1.049$	−0.983
Container	0.572–0.7296	$y = -0.7414x + 0.787$	−0.814
Ro-Ro/Ferry	0.53–0.656	$y = -0.655x + 0.7583$	−0.787

Table 2
Regression equations for the dimensionless L_R according to the ship type. x and y in equation represent C_B and L_R/L_{pp}.

Ship type	Range (C_B)	Linear regression equation ($y = ax + b$)	Correlation coefficient (r)
Tanker	0.81–0.847	$y = -0.6875x + 0.7821$	−0.587
Liquefied gas	0.6973–0.7688	$y = -0.8447x + 0.8244$	−0.627
Bulk carrier	0.82–0.8665	$y = -1.04x + 1.081$	−0.855
General cargo	0.559–0.801	$y = -0.6722x + 0.6952$	−0.988
Container	0.6393–0.7296	$y = 1.247x - 0.6726$	0.991
Ro-Ro/Ferry	0.53–0.5595	$y = 2.731x - 1.28$	0.353

The mean resistance increase of a ship in waves is influenced by many factors related to hull shape, ship operating conditions, wave characteristics, etc. In relation to the nondimensional transfer function of mean resistance increase in regular waves, it is mainly dependent on wave frequency, wave direction, and ship speed, as shown in Eq. (17). Therefore, as shown in Figs. 5–6, the errors of each method were analyzed by classifying them into Froude number (F_n), wavelengths (λ/L), and ship types according to the wave heading (α). For the convenience of analysis, the entire wave heading area in this study is classified into three groups: head seas (180–135 degrees), beam seas (135–45 degrees), and following seas (45–0 degrees). For the detailed formula and application of each method, refer to the original documents (Boom et al., 2013; Lang and Mao, 2020, 2021; Liu and

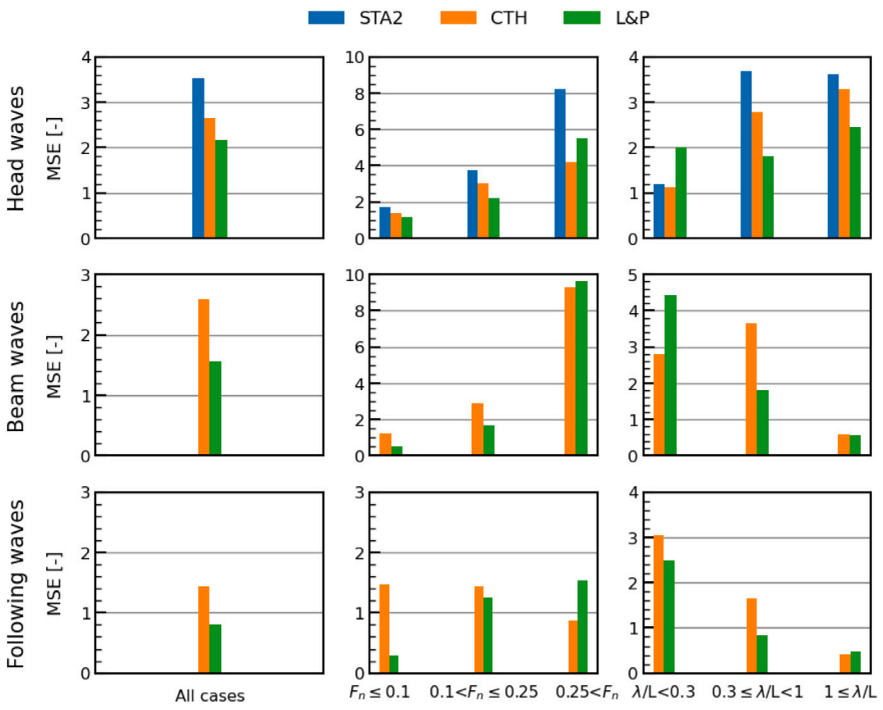

Fig. 5. Comparison of MSE results for added wave resistance methods for all ship types, Froude numbers, and wavelengths. The bar graph in the upper row shows head waves, the middle represents beam waves, and the lower is following waves.

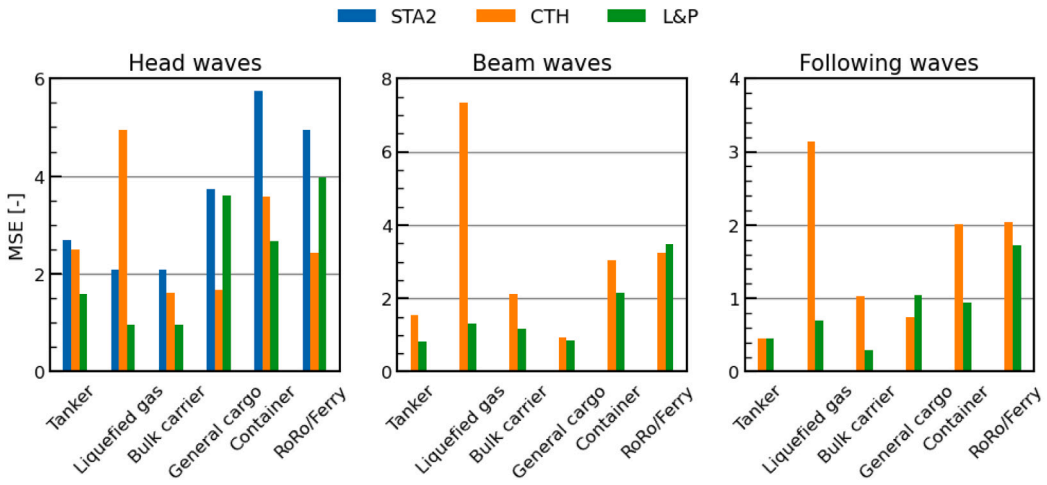

Fig. 6. Comparison of MSE results for added wave resistance methods according to the ship type.

Papanikolaou, 2020)

$$MSE = \frac{1}{n}\sum_{i=1}^{n}(C_{aw_i} - \hat{C}_{aw_i})^2 \tag{1}$$

$$C_{aw} = \frac{R_{aw}}{\rho g \zeta_a^2 B^2/L} \tag{2}$$

where C_{aw} represents the nondimensional transfer function of added wave resistance in regular waves from model test, $\hat{C}_{aw}$ is the estimated value from the semi-empirical method such as STA2, CTH, L&P, and n is the number of samples for the model test belonging to the corresponding classification. R_{aw} is the transfer function of added wave resistance, ρ is the density of water, and g is the gravity acceleration, ζ_a is wave amplitude, B is breadth of the ship, and L is the ship length.

Comparing the overall MSE for each method in head waves, L&P method had the smallest error. However, CTH was noticeably well estimated in the high-speed region of Froude number more than 0.25 and the short waves of less than 0.3 relative wavelengths. In particular, outstanding performance at short waves appears to be the influence of wavelength correction coefficients used in CTH method, which has been adjusted to capture an increase in resistance in the short wave region. The overall MSE of STA2 is about 3.5, which is a relatively larger error than the other two methods, and MSE comparisons as functions of F_n and λ/L also show no better performance than them. This is because, in contrast to the other two approaches, STA2 mainly assumes a general sea trial and does not employ information pertaining to the detailed hull shape when estimating added wave resistance.

In beam seas, overall, L&P had lower MSE than CTH, but similarly to the tendency in head waves, CTH had advantages in high Froude number and short wavelength ranges. In following waves, the absolute peak of added resistance was smaller than that of beam or head sea, and accordingly, the MSE was relatively small. Likewise, L&P showed better performance than CTH in most classifications, but CTH was better in high-speed region.

In terms of error comparison by ship type, the errors of L&P in tanker, liquefied gas, bulk, and container ships were relatively small, while CTH method prevailed in general cargo, ro-ro/ferry ships under head sea conditions. In beam and following wave conditions, except for some cases, L&P had a slightly smaller error than CTH. The difference in error between these two methods is fundamentally due to the introduction of different factors to implement the shape of added wave resistance of a ship. While CTH method modifies the peak position using an encountered frequency correction factor, and the maximum value is derived by using the amplitude adjustment factor, L&P method uses a wave heading-based trigonometric function to estimate the location of resonance frequency and maximum resistance in arbitrary waves. For a more detailed analysis, added resistance according to the wavelength of several cases are plotted in Figs. B1–B3 in Appendix B.

When the prediction results of STA2 against the experimental data in head waves are used as a benchmark, CTH and L&P methods provide significantly smaller MSEs. In addition, since the estimations from the two methods agree fairly well with the experimental data in beam seas and following seas, both are considered to be applicable for estimation of added resistance in the environment of arbitrary waves experienced by ships at sea.

Although L&P method showed a slightly smaller MSE overall compared to CTH, it was not clearly a better method because they showed different performances depending on experimental conditions such as wavelength, wave heading, and ship type. In addition, it is clear that there is still much research that has to be done in this field as the experiments in beam and following sea have relatively greater uncertainty and the amount of data is limited compared to that of head sea.

Therefore, through the analysis of these existing methods, this study sought to develop a model that can ensure good overall performance at arbitrary waves without deviating significantly from model experiment data depending on ship type and various conditions. Here, we intend to apply a method that can reduce errors by properly combining the results of CTH and L&P, which is explained in detail in the next section.

3. Meta model for added resistance in arbitrary waves

3.1. Procedure for developing a combined method

As seen in the previous results, CTH and L&P methods performed relatively better in almost all comparison cases than STA2, and above all, they had the advantage of estimating results for arbitrary wave headings. Comparing CTH and L&P, the difference in performance according to ship type, wavelength, and wave heading was significant. Therefore, this study attempted to develop a new model capable of improving overall performance based on the CTH and L&P methods. Here, a meta-modeling technique was used, which is to create a new model by combining existing models (It will be denoted as a "Combined method" from here). The combined method basically combines the nondimensional added wave resistance coefficients estimated from CTH and L&P to minimize errors with the experimental data. Due to the lack of available model experiment data under irregular wave conditions, it was difficult to develop the model in accordance with various ship conditions.

As a method of blending the two results, a concept similar to R-function used in several previous papers was introduced. Fujii (1975) proposed a method of estimating added resistance due to wave reflection by applying the reflection coefficient (R-function) derived by Ursell (1947) to Havelock's formula, where the R-function was initially designed to extend the effect of wave reflection to relatively long waves. Later, this coefficient was further developed and modified by many other researchers to elaborately address the drift force due to the diffraction effect (Kuroda et al., 2008; Liu, 2020; Mourkogiannis and Liu, 2021). On the other hand, Guo and Steen (2011) adopted a method of multiplying R and 1-R by wave reflection term and ship motion term for the entire wavelength, respectively, to gain the advantage that their contribution to the added wave resistance is smoothly transited from short waves to long waves. Recently, Yang et al. (2018) adopted a more simple and practical tangent hyperbolic function as a blending function instead of a R-function composed of Bessel functions.

In this study, R-function is introduced to combine different theoretical calculations as in Guo and Steen (2011) and Yang et al. (2018), and the tangent hyperbolic function is used because of its simplicity which can smoothly connect the results of the two formulas by adjusting a few coefficients. The transition range of the R-function is extended not only to the wave frequency but also to the wave direction to enable the estimation of added resistance in arbitrary waves. Consequently, the added resistance in arbitrary wave headings can be estimated as described in Eq. (3). The output of the tangent hyperbolic function is between 0 and 1, which is used as the weight of the two methods for the final result. In addition, added wave resistance estimation is performed by classifying it for each ship type to reflect different characteristics caused by the hull shape.

$$R_{wave} = \begin{cases} [1 - f(\alpha)]R_{head} + f(\alpha)R_{beam}, & for \;\; 90 \le \alpha \le 180 \\ [1 - f(\alpha)]R_{beam} + f(\alpha)R_{following}, & for \;\; 0 \le \alpha < 90 \end{cases} \tag{3}$$

where R_{head}, R_{beam}, and $R_{following}$ represent the added wave resistance in head waves, beam waves, and following waves, respectively. $f(\alpha)$ is a function that enables combining the various added wave resistance according to the wave headings as follows:

$$f(\alpha) = \frac{1}{2}[1 + tanh(c(d - \alpha))] \tag{4}$$

$$R_{head}(R_{beam} \; or \; R_{following}) = [1 - g(\lambda/L)]R_{CTH} + g(\lambda/L)R_{L\&P} \tag{5}$$

Here, the coefficient c adjusts the slope of the tangent hyperbolic function and it is divided into c_1 and c_2 according to α as shown in Eq. (6). The coefficient d sets the intermediate position for combining the two results and is divided into 135, 45 degrees according to α value, as seen in Eq. (7). R_{CTH} and $R_{L\&P}$ represent added resistance coefficients estimated from CTH and L&P. By multiplying 1-g and g, which are outputs of tangent hyperbolic function, by R_{CTH} and $R_{L\&P}$, respectively, the two results according to λ/L are smoothly connected.

$$c = \begin{cases} c_1, & for \;\; 90 \le \alpha \le 180 \\ c_2, & for \;\; 0 \le \alpha < 90 \end{cases} \tag{6}$$

$$d = \begin{cases} 135, & for \;\; 90 \le \alpha \le 180 \\ 45, & for \;\; 0 \le \alpha < 90 \end{cases} \tag{7}$$

The values R_{CTH} and $R_{L\&P}$ are combined through the function $g(\lambda/L)$ given in Eq. (8), from which R_{head} (R_{beam} or $R_{following}$) can be estimated.

$$g(\lambda/L) = \frac{1}{2}[1 + tanh(a(b - \lambda/L))] \tag{8}$$

Here, a is a slope coefficient such as c, which is divided into a_1, a_2, and a_3 as shown in Eq. (9). In other words, a serves to determine the slope of the function when combining the results according to λ/L using the combining function, and c is used to combine the results according to α. Coefficient b represents the center position such as d, which is divided into b_1, b_2, and b_3 in Eq. (10).

$$a = \begin{cases} a_1, & for \;\; R_{head} \\ a_2, & for \;\; R_{beam} \\ a_3, & for \;\; R_{following} \end{cases} \tag{9}$$

$$b = \begin{cases} b_1, & for \;\; R_{head} \\ b_2, & for \;\; R_{beam} \\ b_3, & for \;\; R_{following} \end{cases} \tag{10}$$

Fig. 7 displays the combining function and its coefficients in this study as examples. Fig. 7(a) presents the combining function value $f(\alpha)$

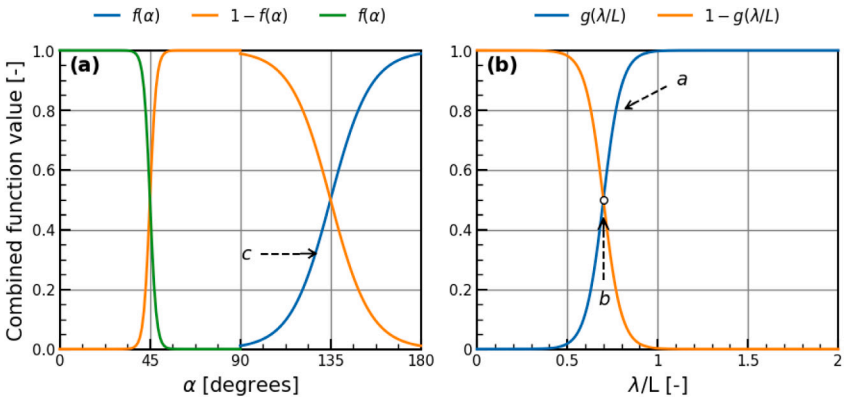

Fig. 7. Coefficients and combining function values according to (a) wave headings, (b) wavelengths proposed in the study.

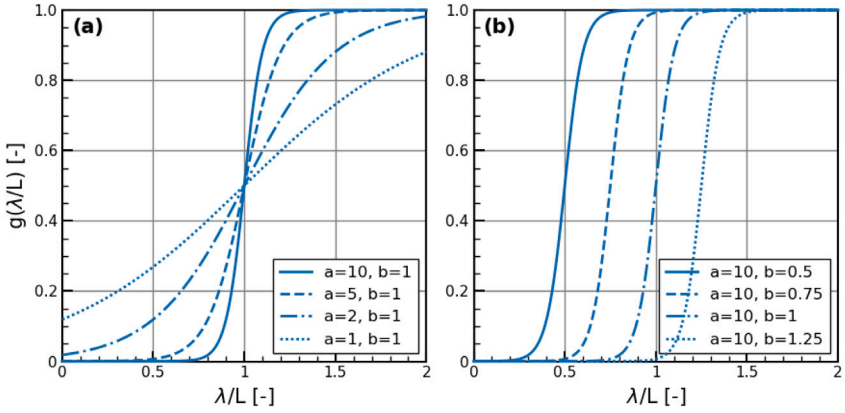

Fig. 8. The results of $g(\lambda/L)$ according to the (a) slope coefficient and (b) center position coefficient. Coefficient c also has the same trend as the results shown in Fig. 8(a) as it is a slope coefficient.

Table 3
The coefficients of combining function according to the ship type. The values in parentheses represent the interquartile ranges of 1,000 bootstrap samples for the coefficients.

Ship type	a_1	b_1	a_2	b_2	a_3	b_3	c_1	c_2
Tanker	−10.00 (1.33)	0.52 (0.13)	7.55 (1.83)	1.08 (0.14)	0.17 (0.34)	1.08 (0.21)	0.04 (0.00)	1.41 (0.53)
Liquefied gas	−9.99 (0.36)	0.26 (0.01)	10.00 (0.01)	2.00 (0.00)	8.16 (1.43)	1.05 (0.10)	−1.2 (0.65)	1.60 (0.54)
Bulk carrier	−1.79 (0.82)	0.59 (0.04)	−0.23 (1.66)	1.84 (0.16)	0.34 (0.10)	1.92 (0.11)	0.00 (0.00)	0.01 (0.02)
General cargo	1.95 (1.01)	0.11 (0.09)	0.92 (0.21)	0.98 (0.07)	0.31 (1.13)	0.74 (0.24)	0.21 (0.39)	0.36 (0.56)
Container	−9.21 (0.77)	0.55 (0.02)	4.52 (1.53)	0.88 (0.13)	2.00 (0.24)	0.95 (0.03)	0.04 (0.00)	−0.08 (0.34)
Ro-Ro/Ferry	−9.35 (0.88)	1.01 (0.03)	−7.91 (1.30)	0.71 (0.15)	6.54 (1.45)	0.84 (0.13)	1.49 (0.50)	0.05 (0.20)

of R_{head}, R_{beam}, and $R_{following}$ according to wave heading, and Fig. 7(b) shows the combining function value $g(\lambda/L)$ of R_a and R_b according to wavelength. As illustrated in Fig. 8, coefficients a and c affect the slope of the combining function value, and coefficient b adjusts where the combining weight is half. As the absolute value of a coefficient increases, the slope of the combining function increases (c has the same trend as a), and as the value of b increases, the center point moves in the direction where λ/L increases.

All the coefficients in Eqs. (6), (9), and (10) were tuned to minimize the error between the model test data and the estimated value from Eq. (3), and in the process, 10 cross-validations with 1000 bootstrap samplings were performed. As a result, the coefficients that provided the smallest errors were obtained through 10 cross-validations per bootstrapping, and 1000 sets of coefficients were finally obtained through 1000 bootstrap sampling. To avoid the influence of some coefficient estimations that deviate extremely from other values, the median value for 1000 bootstrap samples was adopted as the final value of the coefficient in the equation. Table 3 lists the finally obtained coefficient values for each ship type.

3.2. Results of a combined method

In this section, we show how the results of the new method calculated by substituting the coefficients of Table 3 into Eq. (3) are actually applied and how they differ from the CTH and L&P methods. Figs. 9–11 represents the MSE trend of the added wave resistance predictions in head waves, beam waves, and following waves by each method according to the wavelength. As can be seen from the figures, since the coefficients of the combining function are adjusted to minimize the MSE with model experimental data, the results of the Combined method generally tended to follow the method that provided lower MSE for each interval section.

In Figs. 12–13, the results of the Combined method have been added to the previously covered ship cases. According to Fig. 12(a) and Fig. 12(b), the Combined method followed CTH in short waves and L&P method in long waves, and these results were well matched with the actual experimental results, and it was opposite in Fig. 12(c). The reason why different blending trends are shown here is that the coefficients of the combined function are applied differently for each ship type. Moreover, since the Combined method was tuned based on two semi-empirical methods, it had the advantage of being smoothly

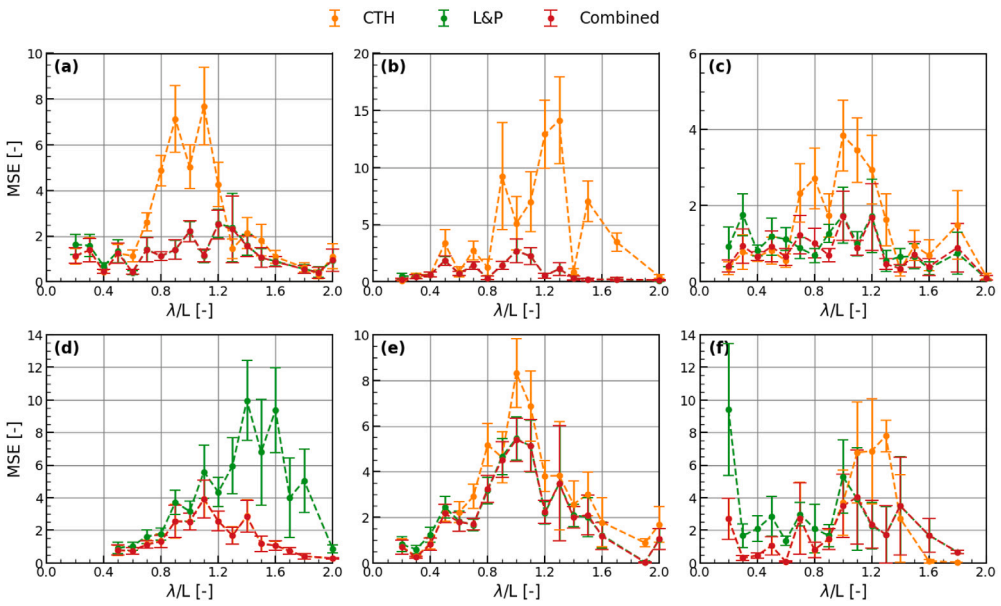

Fig. 9. Comparison of MSE according to wavelengths in head waves. (a) Tanker, (b) Liquefied gas, (c) Bulk carrier, (d) General cargo, (e) Container, (f) Ro-Ro/Ferry. The circle marker stands for the mean of the MSEs of the samples in the corresponding wavelength interval, and the error bar represents the standard error of MSE.

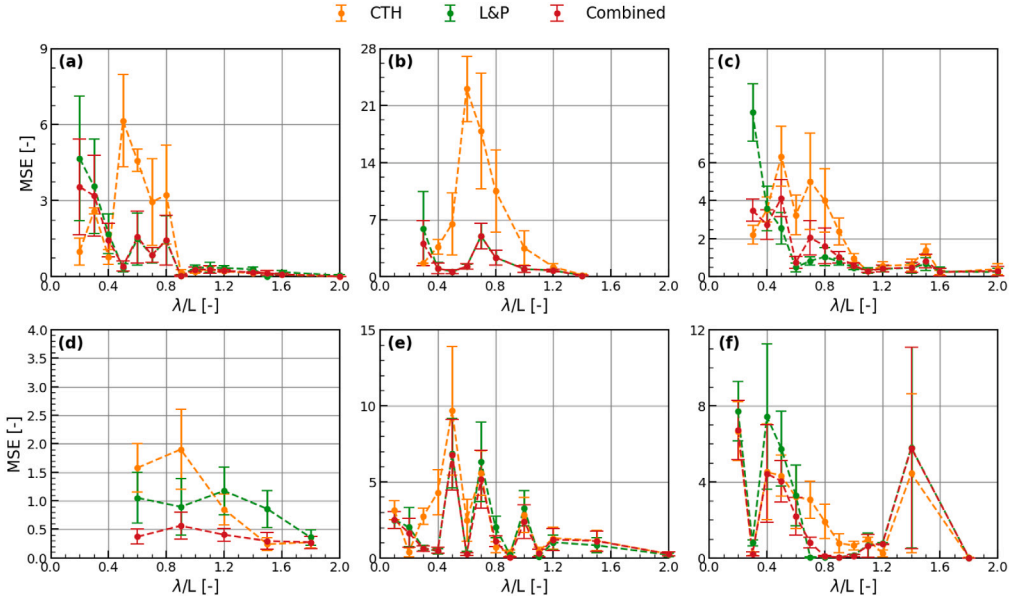

Fig. 10. Comparison of MSE according to wavelengths in beam waves. (a) Tanker, (b) Liquefied gas, (c) Bulk carrier, (d) General cargo, (e) Container, (f) Ro-Ro/Ferry.

connected without deviating significantly from the predicted values of the two methods.

3.3. Analysis of the combined method by experimental data in regular waves

In addition to MSE, several error metrics with correlation coefficient are used to analyze the quality of the predicted value of the Combined method. The Pearson's correlation coefficient (R), Mean Absolute Error (MAE), and Root Mean Squared Error ($RMSE$) are defined as in Eqs. (11)–(13).

$$R_{\mathbf{y},\hat{\mathbf{y}}} = \frac{cov(\mathbf{y},\hat{\mathbf{y}})}{\sigma_{\mathbf{y}}\sigma_{\hat{\mathbf{y}}}} = \frac{E(\mathbf{y}\hat{\mathbf{y}}) - E(\mathbf{y})E(\hat{\mathbf{y}})}{\sigma_{\mathbf{y}}\sigma_{\hat{\mathbf{y}}}} \tag{11}$$

$$MAE = \frac{1}{n}\sum_{i=1}^{n}|y_i - \hat{y}_i| \tag{12}$$

$$RMSE = \sqrt{MSE} \tag{13}$$

where y_i is the true value obtained from the experiment, $\hat{y}$ is the predicted value from the semi-empirical method.

Fig. 14 shows the addition of the results of the Combined method to the MSE comparison bar charts in Section 2.3. It can be seen that the Combined method shows a significantly smaller error compared to STA2 in head waves, and overall MSE is reduced compared to CTH and L&P for all wave headings. It is confirmed that the error of the Combined method is reduced compared to other methods in each section divided according to the Froude number, wavelength, and ship type.

The scatter plots between all experimental data of added resistance in regular waves and the predicted values of STA2, CTH, L&P, and Combined methods are shown in Fig. 16. The best match line of the predictions and experimental values and 30% deviation line from it

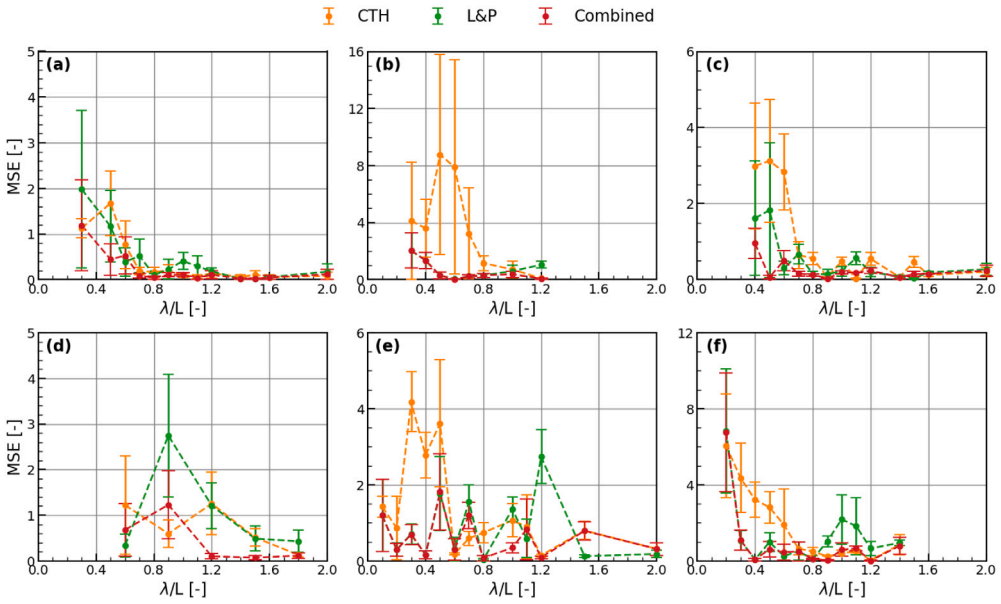

Fig. 11. Comparison of MSE according to wavelengths in following waves. (a) Tanker, (b) Liquefied gas, (c) Bulk carrier, (d) General cargo, (e) Container, (f) Ro-Ro/Ferry.

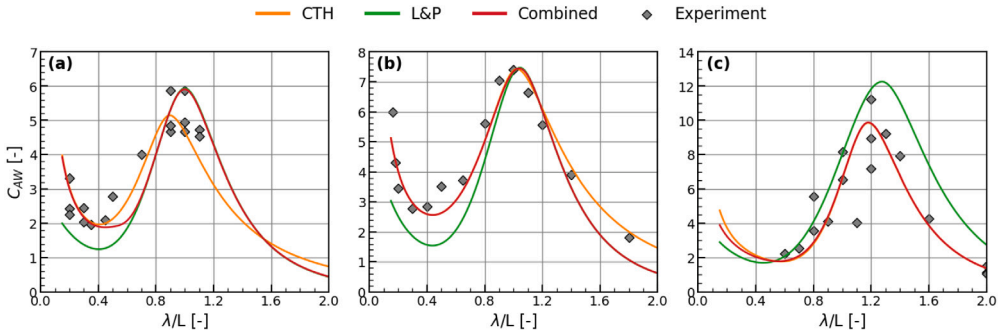

Fig. 12. Examples of Combined method according to the wavelength of (a) DTC, F_n = 0.139, α = 180, (b) HSVA, F_n = 0.232, (c) S60, F_n = 0.283. The figure corresponds to the results of head waves.

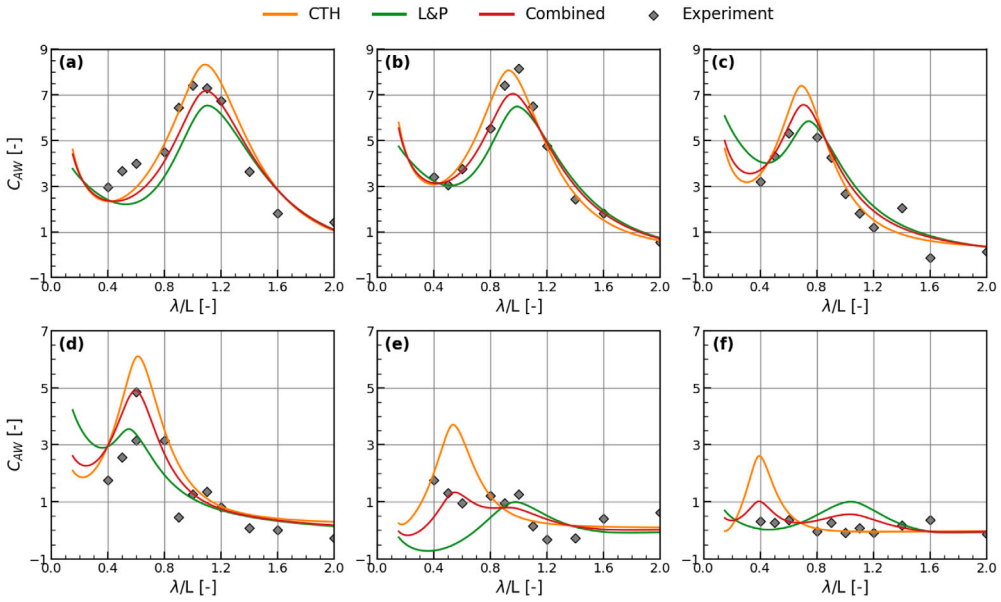

Fig. 13. Examples of Combined method according to the wave heading. 170 k BC, F_n = 0.128 (a) α = 180, (b) α = 150, (c) α = 120, (d) α = 90, (e) α = 30, (f) α = 0.

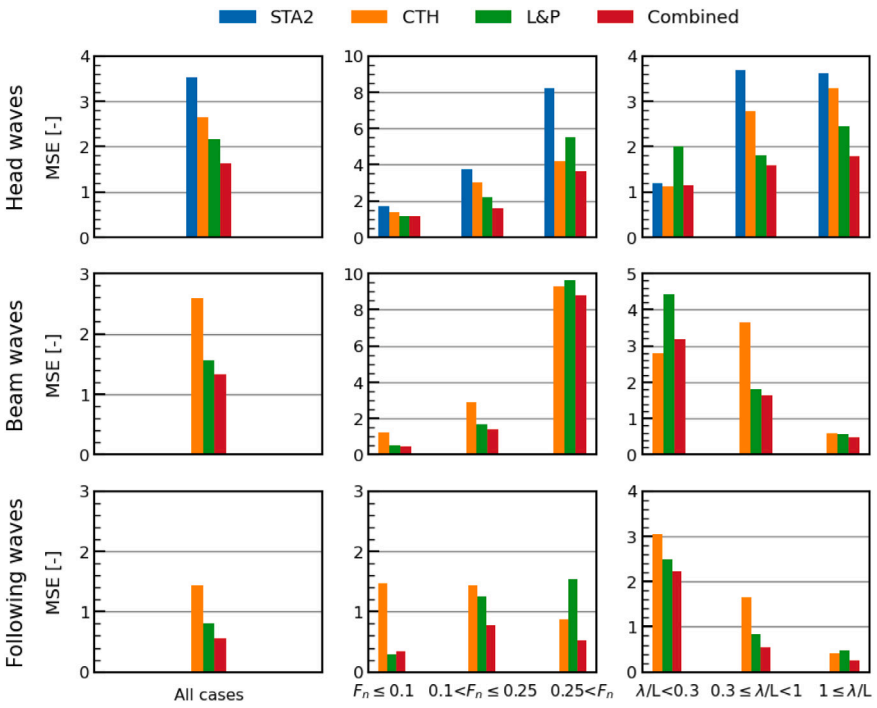

Fig. 14. MSE results of Combined method for added wave resistance according to all cases, Froude numbers, and wavelengths. The bar graph in the upper row shows head waves, the middle represents beam waves, and the lower is following waves.

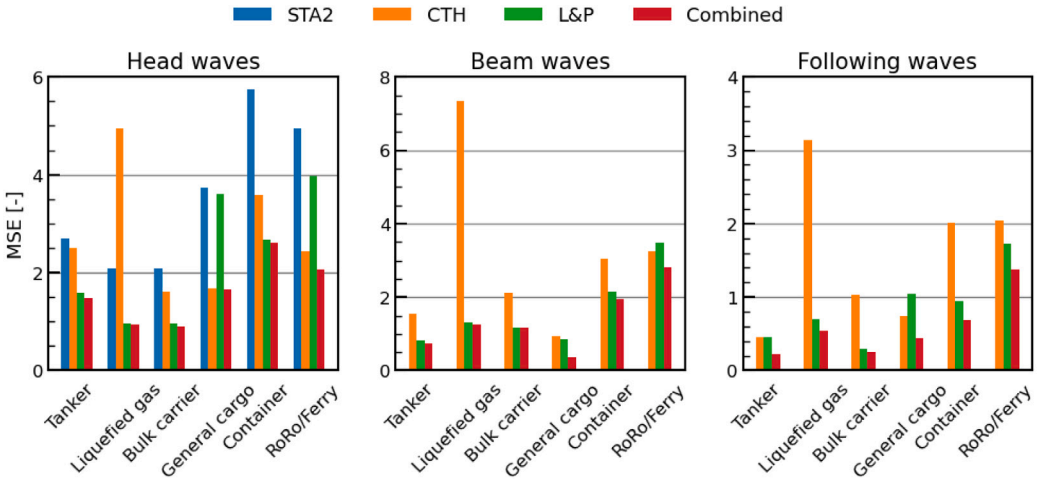

Fig. 15. MSE results of Combined method for added wave resistance according to the ship type.

Table 4
Summary of the components of the correlation coefficients and statistical values for the predicted results in Fig. 16.

Range	Method	R	MAE	$RMSE$
All area	CTH	0.83	1.18	1.63
	L&P	0.87	1.02	1.43
	Combined	0.90	0.89	1.25
Head seas	STA2	0.71	1.44	1.95
	CTH	0.82	1.21	1.66
	L&P	0.84	1.11	1.51
	Combined	0.88	0.96	1.31
Beam seas	CTH	0.68	1.21	1.72
	L&P	0.75	0.94	1.36
	Combined	0.79	0.88	1.27
Following seas	CTH	0.33	0.89	1.23
	L&P	0.59	0.67	0.96
	Combined	0.62	0.53	0.80

are displayed together in the figure. In addition, various error metrics such as MAE, $RMSE$ with R obtained from the corresponding cases are presented in Table 4. For the comparison using scatterplots and the table, refer to those presented by Wang et al. (2021) in a benchmark study organized by ITTC.

As mentioned earlier, STA2 is less accurate in head waves than CTH, L&P, and Combined methods. In particular, as many of the predicted values from STA2 for experimental measurements are located in the lower right side of the figure beyond the 30% deviation line, it is likely to underestimate when added resistance is large. This trend is also in line with the large error of STA2 at high speed and resonance positions in Fig. 14.

On the other hand, the predicted values of CTH and L&P are evenly distributed on both sides of the best match line, and the correlation coefficients are 0.82, 0.84 at head seas, and 0.68, 0.75 at beam seas, showing good correlation for both methods. In following waves, the correlation coefficients are relatively lower at 0.33, 0.59, and many predicted values are observed far outside of the 30% deviation line.

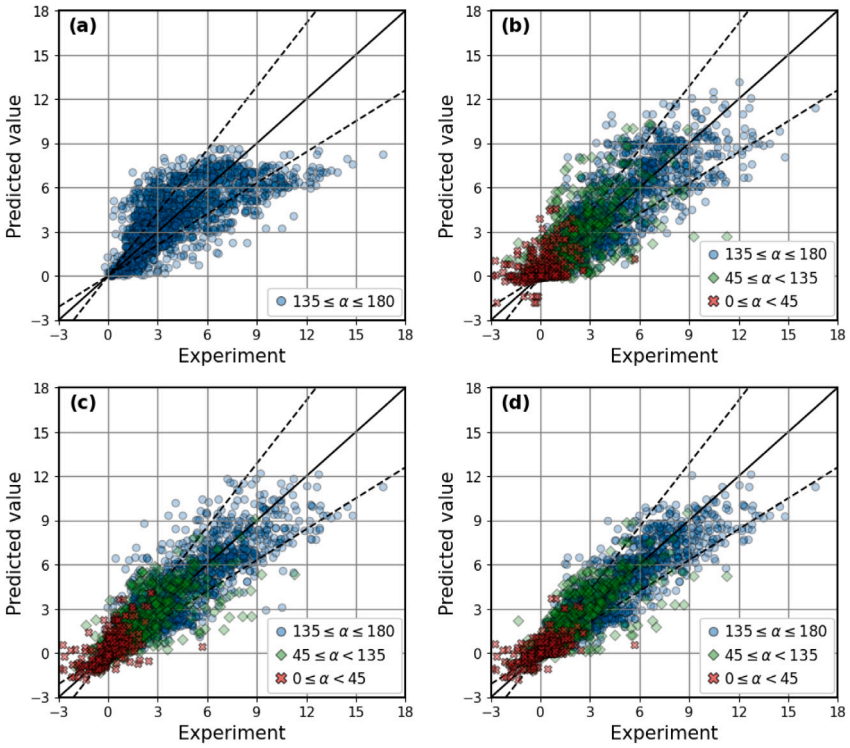

Fig. 16. The scatter plots of the predicted C_{aw} from (a) STA2, (b) CTH, (c) L&P, (d) Combined method against experimental data. The solid line represents the best match line, and dashed line is 30% deviation line from the best match line.

This might be due to the fact that the experimental data in following sea is limited, highly uncertain, and that many values are close to zero. Most of the predicted samples from the Combined method are evenly distributed around the best match line and remain within the 30% deviation line. Compared to the predictions of CTH and L&P, the correlation coefficients of Combined method in all wave directions are higher by 0.62–0.88, and the MAEs are smaller by 0.53–0.96 (see Fig. 15).

4. Observations from comparison of the combined method with full-scale measurements in irregular waves

4.1. Details of full-scale measurements and weather data

In this section, a comparison between the in-service data collected from the two ships and the wave resistance estimated from the Combined method under the corresponding conditions is performed. To this end, not only waves but also the ship resistance factors in calm water, wind, and fouling and roughness conditions, which mainly account for the total resistance of the ship, are obtained through the empirical methods presented in Sections 4.3–4.5. Moreover, the errors between the estimated values of the added wave resistance and the extracted values from the in-service data are compared in Section 4.6.

Table 5 lists the main characteristics of Ship A and Ship B used in the study, and Fig. 17 shows the trajectories of the two ships for the data recording duration. The data of Ship A and Ship B were recorded continuously for 26 months and 2 months from the various fitted sensors and data acquisition systems, and the average values were stored every 15 min and every 1 min, respectively. The collected in-service data of Ship A includes 26 variables and Ship B includes 392 variables. The composition of the data from the two ships is slightly different, but the following variables were commonly used to estimate the resistance components of the ship. Navigation (GPS position, gyro heading, COG heading); Propulsion system (shaft Power, shaft rpm, shaft torque, M/E load); Operating condition (draft, trim, GPS speed, Log speed), etc. The information about the measurement methods of the ship parameters used in this study is shown in Table 6. Additionally, it was possible to extract the data of ships in sea passage operation not at berth or maneuvering by obtaining information on the voyage schedule or navigation state.

In order to calculate the added resistance in wind and waves, information on the surrounding environment the ship experiences during its voyage is required. In this study, weather information such as u and v-components of wind speed, mean wave direction, wave period, and significant wave height was obtained from the re-analysis dataset ERA5 of European Centre for Medium-Range Weather Forecasts (ECMWF), which is a global prediction model and is widely known as one of the most reliable models simulating actual sea weather conditions, instead of onboard measurement (Haiden et al., 2018). There were wind speed and direction data obtained from anemometers installed on ships, but as a result of comparison with wind data from ECMWF, it was found that some parts of the longitudinal wind speed measured from the corresponding ship are changing signs or directions without any probable cause. In addition, there was no data related to waves that could be obtained from the ship.

The horizontal resolution of the dataset is provided based on a grid of $0.25° \times 0.25°$ for atmosphere and $0.5° \times 0.5°$ for ocean waves, respectively, and the temporal resolution of it is hourly. The weather data at the closest position and time grid can be obtained by matching each data sample of the ship with data from the ECMWF. Through the sequential interpolations on weather data according to the location and timestamp of the ship, the actual environment encountered by the ship can be extracted. It is used as an input value for calculating added resistance, and Figs. 18–19 display distributions of wind speed and significant wave height during the data collection periods.

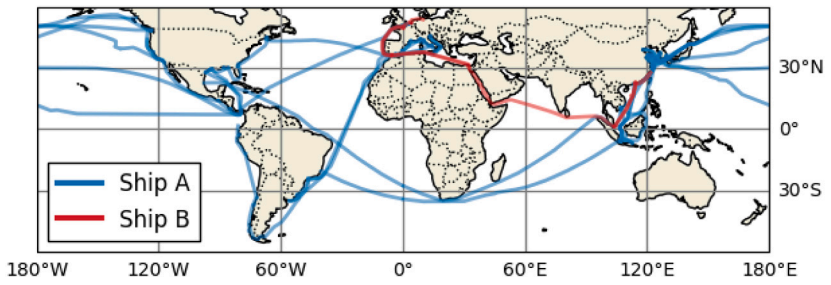

Fig. 17. Operational routes of Ship A and B for the data recording duration.

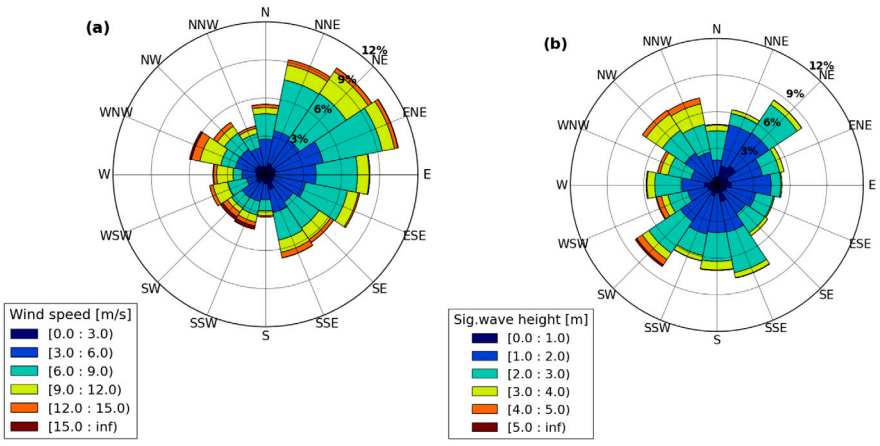

Fig. 18. The distribution plots of (a) wind, (b) waves encountered by Ship A. Figure (a) shows the degree of wind occurrence according to the true wind direction in %. The color sector shows the true wind speed in m/s. Figure (b) represents the degree of waves occurrence according to the wave direction in %. The color sector shows the significant wave height in meters. (For interpretation of the references to color in this figure legend, the reader is referred to the web version of this article.)

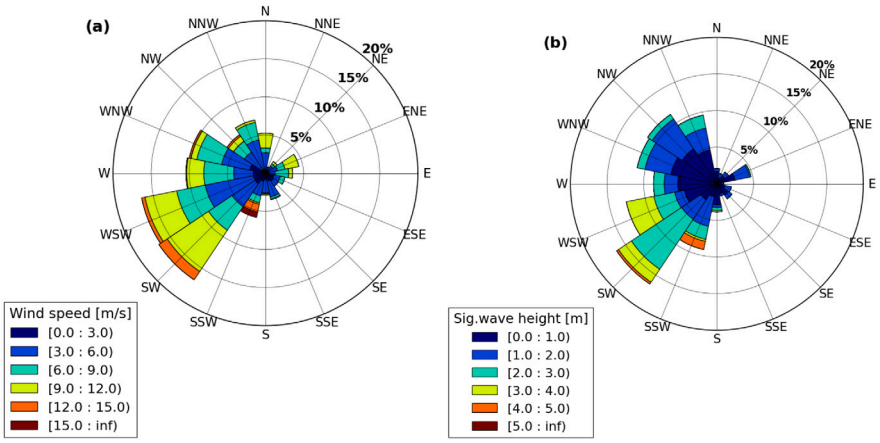

Fig. 19. The distribution plots of (a) wind, (b) waves encountered by Ship B. (For interpretation of the references to color in this figure legend, the reader is referred to the web version of this article.)

4.2. Data pre-processing

Raw measurement data includes all types of navigation status, such as accelerating, decelerating, maneuvering, and even in port. To perform accurate speed-power performance analysis, it is necessary to extract the data sections in which the ship operates steadily. In this study, the steady-state detection algorithm proposed by Dalheim and Steen (2020) was applied. This algorithm identifies a change point among the samples by using a sliding window and its corresponding t-value of the local slope. The slope of the fitted regression line from the regression analysis is used to check the unsteady state. In addition, sections with propeller speed below a certain limit were considered to be in the state of maneuvering. The voyage classification of data samples to which steady-state detection and filtering are applied is shown as an example in Fig. 20. As a result, Figs. 21–22 show the histograms of speed through water, propeller speed, mean draft, and engine power for the pre-processed data of Ship A and Ship B.

4.3. Estimation of ship resistance factor by empirical approaches

In general, the resistance components that account for most of the total resistance of a ship are calm water resistance, added resistance due to wind, and added resistance in waves. The effects of drifting and rudder on added resistance are neglected in this study. To extract the contribution of the added wave resistance to the power demand from in-service data, the resistance in calm water conditions

Table 5
Main dimensions and information of ships used in the study.

	Ship A	Ship B
Ship type	General cargo	Container
Length [m]	194	350
Breadth [m]	32	48
Block coefficient [-]	0.79	0.66
Radius of pitch gyration [-]	0.25	0.25
Deadweight tonnage [ton]	12.6	14.5
Maximum continuous rating [kW]	10780	65640
Design draft [m]	12.6	14.5
Service speed [knots]	15.5	24.7

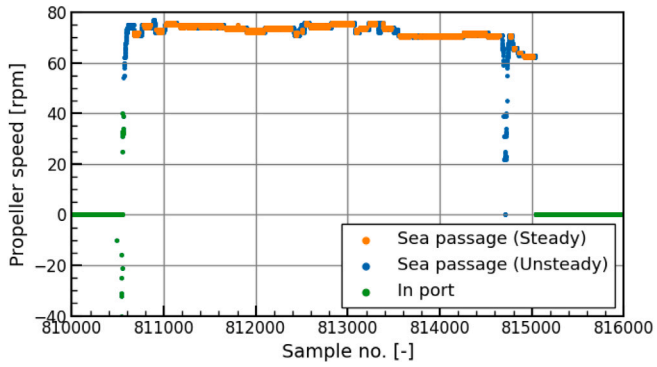

Fig. 20. Classification of voyage status according to propeller speed. It shows an example of one short voyage data.

and added resistance due to wind, were considered as expressed in Eqs. (14)–(15).

$$R_{total} = R_{calm} + R_{wind} + R_{wave} \tag{14}$$

$$P_B = \frac{R_{total} \cdot V}{\eta_T} \tag{15}$$

where R_{total} is the total resistance of a ship, R_{calm} is calm water resistance, R_{wind} is the added resistance due to wind, η_T is the overall efficiency, and P_B is engine brake power.

Here, the frictional coefficient was obtained from ITTC-1957 correlation line, and the residual resistance coefficient was calculated using Hollenbach's method (1998) since it was found that Hollenbach's method fits relatively well for the given ship. It was developed based on regression analysis of 433 relatively modern ship models, requiring basic ship design parameters such as length, breadth, draft, displacement, wetted surface area, block coefficient, and propeller diameter for the calculation. According to the original paper, Hollenbach's method had a relatively lower standard deviation of the error in resistance against its validation test cases compared to Holtrop–Mennen (1984), Guldhammer (1974), Lap-Keller (1973), and Series-60 (1972).

Due to changes in hull roughness caused by marine fouling, differences in powering performance may occur during the operational period, and such differences should be additionally corrected as a roughness allowance. The roughness allowance (ΔC_F) can be calculated as the difference between the total resistance coefficient of in-service data ($C_{T,Data}$) filtered by wind speeds less than 5.5 m/s, where calm water resistance dominates, and the total resistance coefficient in the same conditions obtained from empirical methods ($C_{T,Emp}$) as shown in Eq. (16) (Gupta et al., 2021). $C_{T,Data}$ represents the total resistance coefficient due to calm water resistance as well as the added resistance due to the wind and waves and fouling, while $C_{T,Emp}$ denotes the total resistance coefficient due to calm water resistance, added resistances due to wind and waves without taking fouling into account. Therefore, it is assumed that only fouling contribution is left after the subtraction. Furthermore, trends of roughness allowance were observed over cumulative static time between specific hull cleaning events, and a fitted trend line is used as a corrected roughness allowance (ΔC_F), as shown in Fig. 23(c). The overall operating speed range of the two ships used in this study was about Froude number 0.09 to 0.18, the impact of the speed of the wave-making resistance coefficient or viscous resistance coefficient within this range is not that significant, thus the corresponding resistance coefficients, which are less than Froude number 0.2 is assumed to be constant.

$$\Delta C_F = C_{T,Data} - C_{T,Emp} \tag{16}$$

There were a total of four propeller and hull cleaning events of Ship A in 2.5 years, and the roughness allowance was estimated considering this. In case of the Ship B, there was no specific data related to fouling and roughness such as cleaning event history. Since the berthing time of the container ship was relatively short, and data of one voyage (approximately 2 months) was used, it was assumed that there would have been no significant change in the hull roughness during the period. As a result, the typical average hull roughness of an operating ship, 150 μm, was applied for the estimation of the roughness allowance according to MARINTEK's formula (Minsaas, 1982; Steen and Aarsnes, 2014).

The wind resistance coefficient was estimated from the regression formula developed by Fujiwara (2006), and the resistance increase due to relative wind was calculated according to the method recommended by ISO 15016 (2015). Wind affected areas of the hull were calculated based on the depth and draft of Ship A and B. Since the wind-affected area above the water surface of Ship A is mainly an accommodation area, the upper structure according to the draft of the ship was estimated using a detailed hull shape. Meanwhile, the container ship has not only accommodation areas but also cargoes on the deck, and since there was no detailed information on cargo volume and arrangement, the parameter estimation method from Kitamura et al. (2017) was used for the above-water structure area for Ship B.

Finally, the relevant resistance components of each ship obtained through the previous estimation process are shown in Figs. 23–24. In the case of Ship B, the figure related to the roughness allowance is not included as it was assumed to be constant. The detailed process to estimate added wave resistance is covered in the next section.

4.4. Wave spectrum and response amplitude operator in regular waves

The mean resistance increase in short-crested irregular waves (R_{wave}) can be calculated as a linear superposition of the transfer function of added resistance in regular waves (R_{aw}) and directional wave spectrum (E), as expressed in Eq. (17). The transfer functions of added resistance in regular waves according to different speeds for the subject ships estimated from the Combined method are shown in the following Figs. 25–26.

$$R_{wave} = 2\int_0^{\frac{\pi}{2}}\int_0^{\infty} \frac{R_{aw}(\omega,\alpha;V)E(\omega,\alpha)}{\zeta_a^2} d\omega d\alpha \tag{17}$$

The directional spectrum is not measured in this study, standard frequency spectrum (S) with the angular distribution function (G) is considered as in Eq. (18).

$$E(\omega,\alpha) = S(\omega)\cdot G(\alpha) \tag{18}$$

There are various wave spectra representing different characteristics depending on the location and environment of the ocean. In this study, the modified Pierson–Moscowitz spectrum of ITTC 1978 (2017), commonly used for the open ocean, is applied through the process as shown in Eqs. (19)–(21).

$$S(\omega) = \frac{A}{\omega^5}\exp\left(-\frac{B}{\omega^4}\right) \tag{19}$$

$$A = 173\frac{H_s^2}{T_m^4} \tag{20}$$

Table 6
Measurement methods of the ship parameters used in the study.

Parameter	Measurement device	Unit
Position	DGPS	latitude, longitude
Heading	Gyro compass	degree
Course over ground	DGPS	degree
Speed over ground	DGPS	knots
Speed through water	Doppler speed log	knots
Shaft power	Shaft horsepower meter	kW
Shaft revolutions	Ship revs counter	rev/min
Draft	Draft gauges	meter
Weather information	ECMWF ERA5 reanalysis	Temporal resolution: hourly
		Horizontal resolution: 0.25° × 0.25° (atmosphere)
		Horizontal resolution: 0.5° × 0.5° (Ocean waves)

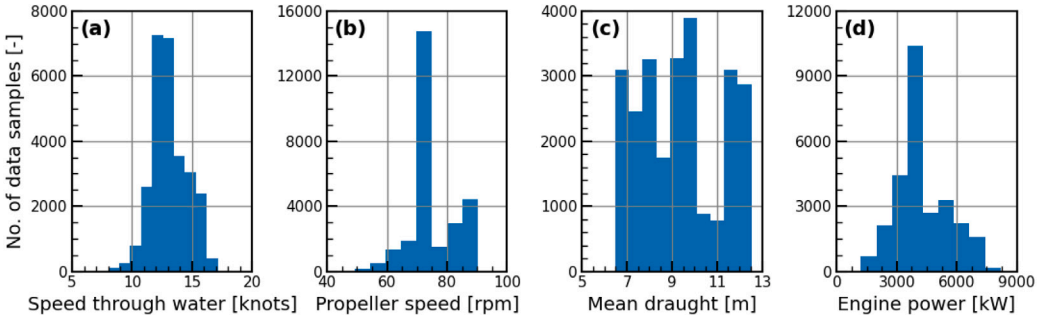

Fig. 21. Histograms of (a) speed, (b) main engine rpm, (c) mean draft, and the (d) engine power of Ship A for the data recording duration.

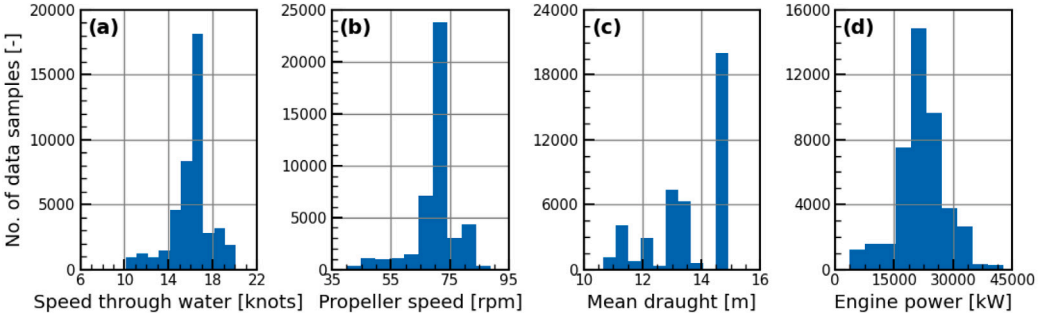

Fig. 22. Histograms of (a) speed, (b) main engine rpm, (c) mean draft, and the (d) engine power of Ship B for the data recording duration.

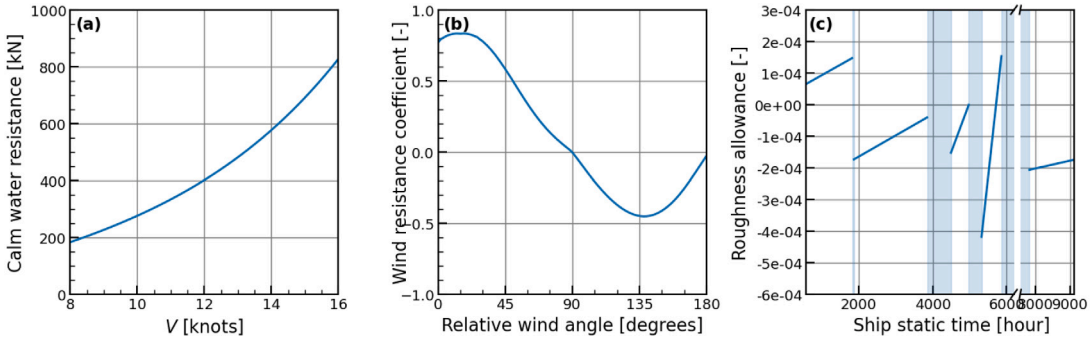

Fig. 23. Ship resistance components for Ship A: (a) calm water resistance, (b) wind resistance coefficient, (c) roughness allowance. The resistance factors in Figures (a) and (b) are calculated based on the design loading condition. The blue shaded part in (c) is propeller cleaning event, and the solid line shows the trend line of mean roughness allowance according to the ship static time. (For interpretation of the references to color in this figure legend, the reader is referred to the web version of this article.)

$$B = \frac{691}{T_m^4} \tag{21}$$

where ω is the circular wave frequency, H_s is the significant wave height, and T_m is the mean wave period.

For the angular distribution function for the wind waves, the cosine-power type is applied such as in Eq. (22), and the spreading parameter is set to 1 (ITTC, 2017)

$$G(\alpha) = \begin{cases} \frac{2^{2s}}{\pi} \frac{\Gamma^2(s+1)}{\Gamma(2s+1)} cos^2(\theta - \alpha), & -\frac{\pi}{2} \le \theta - \alpha \le \frac{\pi}{2} \\ 0, & otherwise \end{cases} \tag{22}$$

where θ is the primary wave direction, s is a directional spreading parameter, and Γ is a Gamma function.

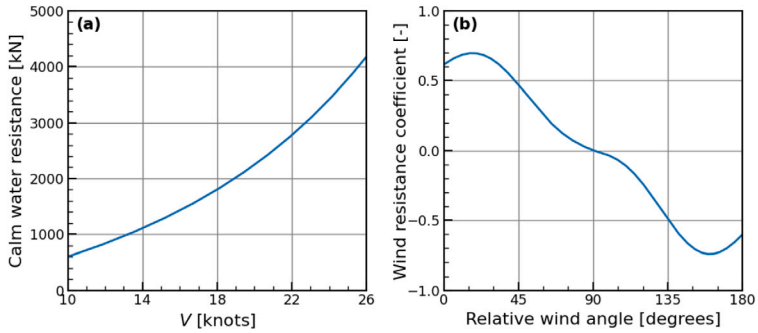

Fig. 24. Ship resistance components for Ship B: (a) calm water resistance, (b) wind resistance coefficient.

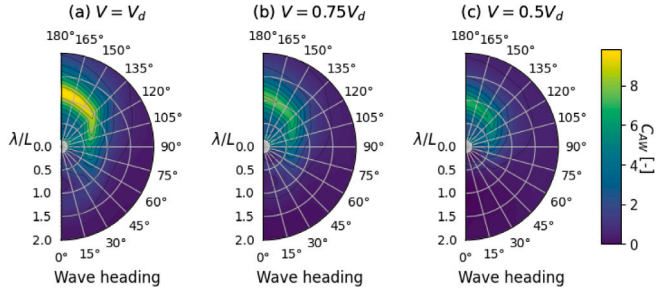

Fig. 25. Comparison of added resistance coefficient in regular waves of Ship A at (a) $V = V_d$, (b) $V = 0.75V_d$, (c) $V = 0.5V_d$ computed using Combined method. V_d represents the design speed, and the results of the figures are based on the design loading condition of the ship.

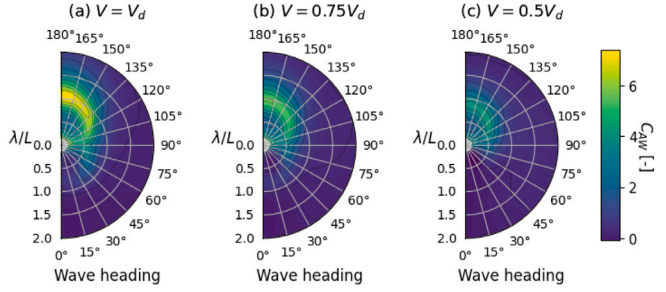

Fig. 26. Comparison of added resistance coefficient in regular waves of Ship B at (a) $V = V_d$, (b) $V = 0.75V_d$, (c) $V = 0.5V_d$ computed using Combined method.

4.5. Comparison of semi-empirical methods in irregular waves

Theoretical estimations for added resistance in irregular waves of Ship A and Ship B by various methods are plotted in Fig. 28 and Fig. 29, respectively, in which sensitivity analysis according to significant wave height (H_s), mean wave period (T_m), wave heading (α), and ship speed (V) is performed. The reference conditions for the comparative case of Ship A are $H_s = 1$ m, $T_m = 10$ s, $\alpha = 180$, and $V = 15.5$ knots, and Ship B are $H_s = 1$ m, $T_m = 12$ s, $\alpha = 180$, and $V = 24.7$ knots. It is assumed that the remaining conditions are constant while analyzing variation for each parameter. Basically, the added resistance in irregular waves is calculated through the process of Section 4.4, and the RAOs of the two ships under the reference conditions are shown in Fig. 27. For the comparison in irregular waves, not only STA2, CTH, and L&P but also Shopera and Kreitner's methods that can directly calculate the added resistance in irregular waves are added. The CTH, L&P, and Combined methods take into account the angular distribution function in estimating added resistance in irregular waves as shown in Eq. (17), while for Shopera and Kreitner the angular distribution function is not applied, since these methods work directly with irregular waves, so a normal directional spreading is presumably included in the methods. Since STA2 is applicable to the mean resistance increase in long crested irregular head waves according to the original intention, the angular distribution function in Eq. (18) was not used.

According to the study of Lang and Mao (2021), it was found that the added resistance rose more drastically as the significant wave height increased compared to the linear superposition. In their work, a wave height correction factor ($C_{H_s} = \sqrt[3.5]{H_s}$) was established that can be used to account for the effects of higher resistance brought on by a large vessel's motion as well as decreased propulsion efficiency in rough seas. This correction is reflected by multiplying the added resistance due to waves (R_{wave}) by the wave height correction factor (C_{H_s}), and Its effectiveness in minimizing errors between full-scale measurements and estimated values from the semi-empirical method has been shown. In this study, since the Combined method basically implemented the CTH method in its original form, the wave height correction factor was applied to the CTH method also when it was used as part of the Combined method.

Wave resistance over the significant wave height

As the significant wave height increased, added resistance due to waves tended to increase very steeply. In particular, the difference in results between methods at a height of 2 m or more was noticeable. For the considered ships A and B, the results of the Combined, CTH methods, and STA2 were the largest. In both cases, the Shopera and L&P methods provided similar results, while the Kreitner provided smaller values compared to the other methods.

Wave resistance over the mean wave period

STA2, CTH, L&P, and Combined method formed a peak at around 8–9 s for Ship A and 11–12 s for Ship B, and considering the actual length of the ships, it seemed to match with the resonance frequency positions properly. In addition, weak local crests were formed at around 4–6 s and 5–7 s, respectively, which was interpreted as reflecting the increase in added resistance at a short wavelength. The Combined method seemed to properly reflect the characteristics of CTH and L&P methods according to the mean wave period. Shopera and Kreitner methods showed constant results over the mean wave period, as expected. Since they focus on estimating maximum added wave resistance and do not include the mean wave period in the formula, Shopera provided similar results as the maximum values seen from CTH, L&P, Combined methods, and STA2, while Kreitner had values less than that.

Wave resistance over the wave heading

Since Shopera, Kreitner, and STA2 only consider added wave resistance in head waves, it was assumed that STA2 and Kreitner provided the same values at wave headings from 135 to 180 degrees, and from 150 degrees to 180 degrees for Shopera. Moreover, their results in beam and following waves were set to zero. According to the estimated results from CTH, L&P, and Combined method, the maximum added resistance occurred in head waves, and the magnitude became smaller as it went to the stern direction. It can be seen that the added resistance in the range between 180 degrees and 135 degrees decreased slightly, then

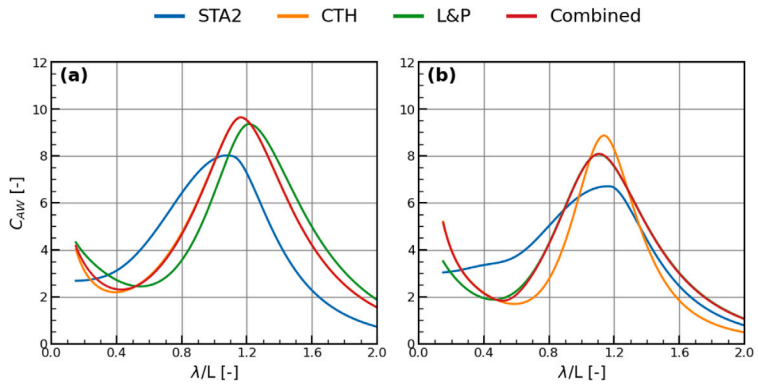

Fig. 27. Added resistance coefficient in regular waves of (a) Ship A (α = 180, V = 15.5 knots), (b) Ship B (α = 180, V = 24.7 knots).

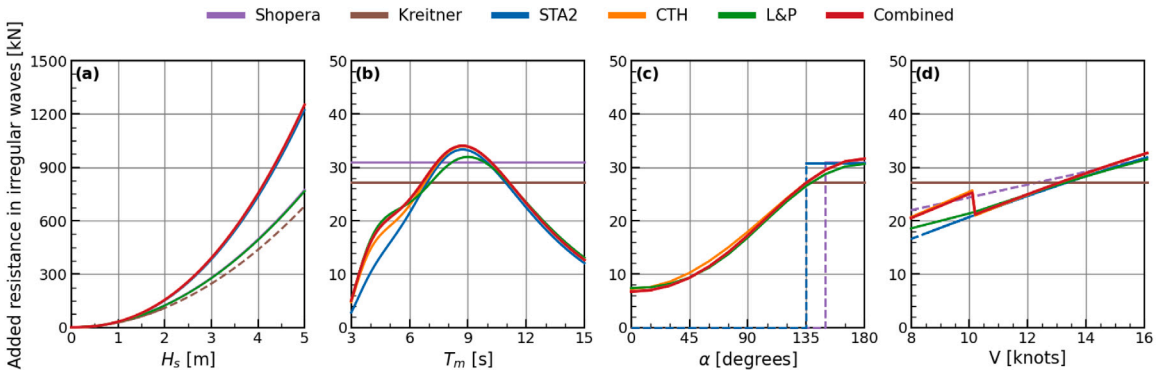

Fig. 28. Added resistance of Ship A in irregular waves against (a) significant wave height, (b) mean wave period, (c) wave heading, (d) vessel speed according to various estimation methods. The y axis represents added resistance in irregular waves, and the section indicated by the hatched line is the range beyond the restriction of the corresponding method (Reference conditions: H_s = 1 m, T_m = 10 s, α = 180, V = 15.5 knots).

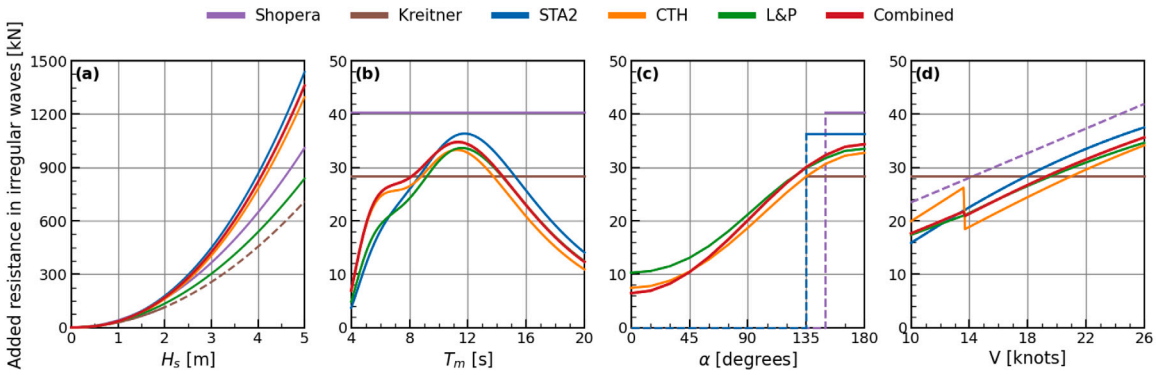

Fig. 29. Added resistance of Ship B in irregular waves against (a) significant wave height, (b) mean wave period, (c) wave heading, (d) vessel speed according to various estimation methods (Reference conditions: H_s = 1 m, T_m = 12 s, α = 180, V = 24.7 knots).

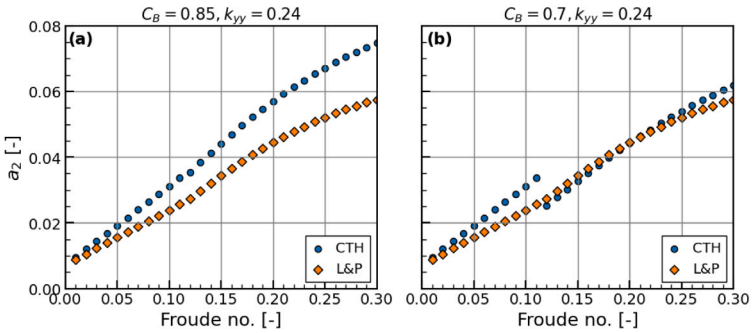

Fig. 30. Speed correction factor (a_2) according to Froude no. at (a) $C_B = 0.85$, $k_{yy} = 0.24$, (b) $C_B = 0.7$, $k_{yy} = 0.24$.

in the range between 135 degrees and 0 degrees dropped sharply. The Combined method seemed to follow the results of the two methods, which were properly weighted for the wave headings. In head waves, STA2, Shopera provided similar resistances to CTH, L&P, and Combined method, and Kreitner tended to underestimate significantly compared to other methods.

Wave resistance over the speed of the ship

Most methods showed a trend of almost linearly increasing added resistance in proportion to speed. CTH showed a drop in resistance at a certain speed, which was found to be due to the influence of the a_2 coefficient used in wave motion-induced added resistance. Since the calculation of a_2 in the CTH method is different for Froude number smaller and larger than 0.12, where block coefficient (C_B) and pitch gyration (k_{yy}) were introduced in the a_2 equation only at $F_n = 0.12$ or higher, it turned out that some combinations of C_B and k_{yy} result in a discontinuous a_2 as function of F_n. This trend can be seen from the comparison results of the speed correction factor between the two methods according to Froude number in Fig. 30. Meanwhile, the Kreitner method estimated a constant value according to the ship speed, which was larger or smaller than the other methods depending on the speed. The Combined method mainly followed the CTH method in the case of the general cargo ship and the L&P method for the container ship. As the Combined method integrates the results of the two methods, the discontinuity of added resistance as a function of F_n occurring in the CTH method may be visible in some cases.

4.6. Observations from comparison of the combined method with full-scale measurements

In this section, the results of the combined method were compared with using full-scale measurement data of ships A and B. As shown in Eq. (15), the brake power of the ship is estimated by considering the ship resistance factors, propulsive efficiency, and speed. It is compared with the main engine power measured from the shaft horsepower meter on-board.

Figs. 32 and 33 show the percentage of absolute error between the measured power (P_{MEAS}) and the estimated power (P_{EST}) for each parameter (H_s, T_m, α, V), and it is calculated according to Eq. (23). Fig. 31 shows an example of the confidence interval, mean line, and histogram for the error of the data samples. The shadowed range in the figure is the confidence interval of 95% mean for the samples, which represents the range of values that there is a 95% probability that the mean value of the samples falls within. The collected data of each parameter were divided at regular intervals to obtain the error defined in Eq. (23) for the samples for each section. In addition, the confidence interval and mean line representing each section were estimated, and they were connected. Here, "no correction" means that added resistance due to waves is not included in the total estimated power.

$$Error\ of\ power\ prediction\,[\%] = \frac{|P_{MEAS} - P_{EST}|}{P_{MEAS}} \times 100 \tag{23}$$

Error trend over the significant wave height

From Fig. 32(a) and Fig. 33(a), it can be seen that for a significant wave height of 1 m or less, there is little difference in error between the methods, including the "no correction". This is as expected since the added resistance is a small fraction of the total for small waves. At a significant wave height of 1 m or more, the difference between "no correction" and the other correction methods is clearly visible. Since there were not many data samples in the range between 3 m to 4 m, uncertainty was included in the error trend, but the relative performance difference of each method can be distinguished. It can be seen that the Combined method gives the smallest error compared to the other methods over the entire H_s range, with values in the range 7%–20%, while CTH and L&P show an error of about 10%–25%. The errors of Kreitner, Shopera, and STA2 methods show much larger errors than these.

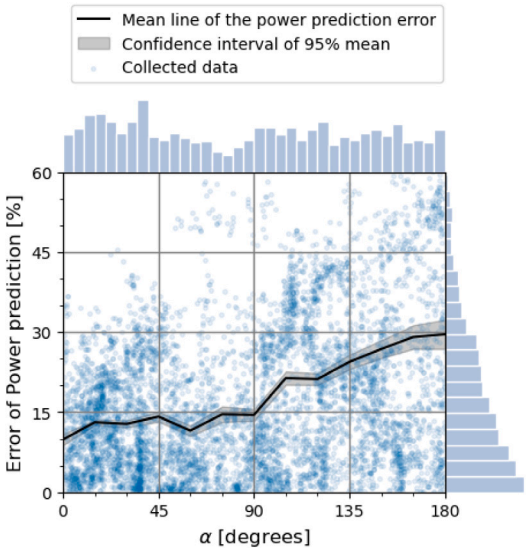

Fig. 31. An example showing the power prediction errors of collected samples with the histogram and confidence interval. It corresponds to the case of the "no correction" according to wave headings of Ship A (Refer to Fig. 32(c)). The solid line indicates the mean line of the power prediction error, shadowed area represents its confidence interval of 95% mean, and marker is the collected data.

Error trend over the mean wave period

The error plotted as a function of the mean wave period in Fig. 32(b) and Fig. 33(b) ranges from 8 to 26% over the entire range, which is somewhat smaller than for the other parameters. Compared with "no correction", the effect of wave correction can be identified for periods larger than 5 s for Ship A and 7 s for Ship B. It can also be seen that the errors of CTH, L&P, and Combined methods are significantly smaller in the vicinity of the peak compared to other methods.

Error trend over the wave heading

Since Shopera, Kreitner, and STA2 are applicable only to head waves, they have the same error as "no correction" in following and beam waves. The errors of CTH, L&P, and Combined methods differ significantly in the range between 60 to 135 degrees compared to other methods. The Combined method gives the smallest error over most of the heading range. However, the increase of propulsion power due to waves of Ship A and Ship B in the range of 0–30 degrees and 0–45 degrees, respectively, seems to be almost insignificant.

Error trend over the speed of the ship

Looking at the error trends over the speed in Fig. 32(d) and Fig. 33(d), the relative effect of wave correction on the propulsion power generally decreases as the speed of the ship increases, which indicates that added resistance increase less rapidly with speed than the calm water resistance. The Combined method shows a similar error trend as CTH for the general cargo ship and as L&P for the container ship and provides generally good performance for all speeds.

Fig. 34(a) shows $RMSE$ of power prediction by each method for the entire in-service data, and Fig. 34(b) represents the relative $RMSE$, of which all the $RMSE$ results are normalized based on the $RMSE$ of Combined method to identify the relative error degree of each method. The error metrics used in Fig. 34 are defined in Eqs. (24)–(25). Since Fig. 28 and Fig. 29 show theoretical results of added resistances assuming specific conditions, and Figs. 32 and 33 represent the error of the predicted value for the actual data in all operating conditions, the results of those figures might give slightly different levels of agreement

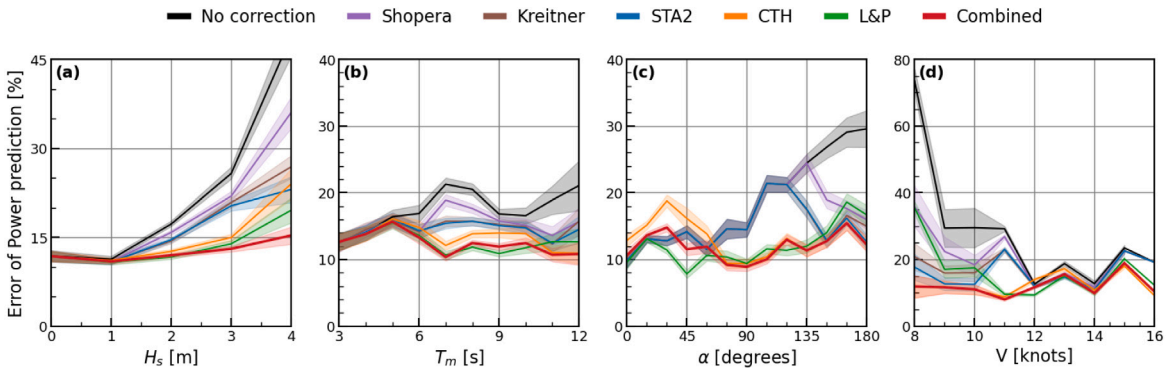

Fig. 32. Power prediction error of Ship A against (a) significant wave height, (b) mean wave period, (c) wave heading, (d) vessel speed according to various estimation methods. The y axis represents the absolute errors between the measurements and the estimation as a percentage.

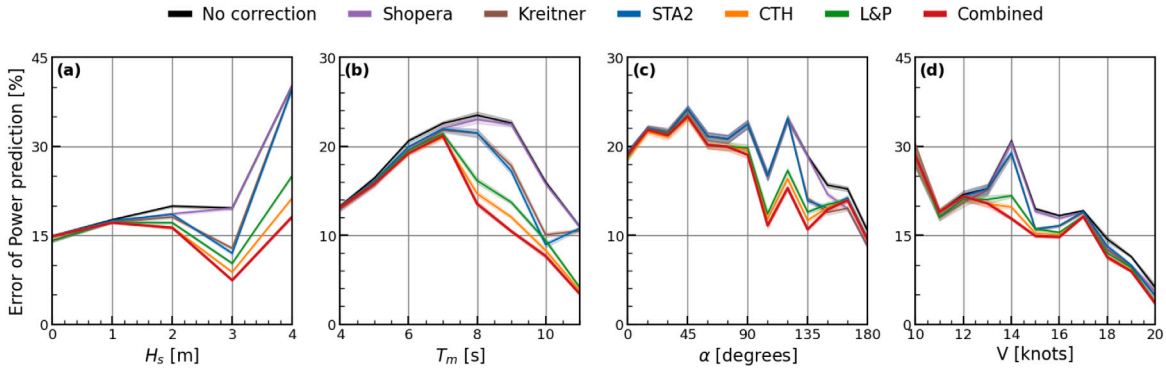

Fig. 33. Power prediction error of Ship B against (a) significant wave height, (b) mean wave period, (c) wave heading, (d) vessel speed according to various estimation methods.

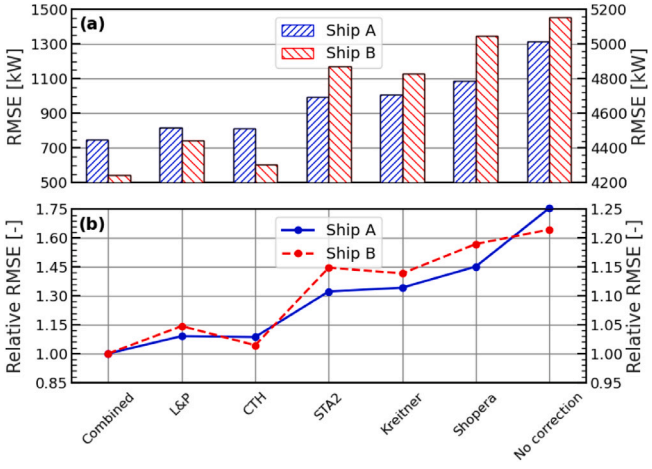

Fig. 34. Error analysis against full-scale measurements for Ship A. Figure (a) and Figure (b) show $RMSE$ and relative $RMSE$.

between the different methods.

$$RMSE\ of\ power\ prediction = \sqrt{\frac{1}{n}\sum_{i=1}^{n}\left(P_{MEAS,i} - P_{EST,i}\right)^2} \tag{24}$$

$$Relative\ RMSE = \frac{RMSE_{Empirical}}{RMSE_{Combined}} \tag{25}$$

where $RMSE_{Empirical}$ is the $RMSE$ of the selected empirical method, and $RMSE_{Combined}$ is the $RMSE$ of the Combined method.

It is confirmed that the correction of the propulsion power due to waves is large and strongly varying as function of V, H_s, α, and T_m within the range of the collected data used in the study. Referring to Fig. 34, Relative $RMSE$s on the two ships show a similar trend depending on the overall method, although there is a difference in the value. Compared to the $RMSE$ of the Combined method, Ship A showed about 30%–45% larger errors for Kreitner, Shopera, and STA2 and about 8%–9% for CTH and L&P, while Ship B had 14%–19% and 1%–5% larger errors. Although we did not list the results here, applying the wave height correction factor also to the L&P method was effective in reducing errors against in-service data that we collected. However, we decided not to include the wave height correction to the L&P method, since it is not part of that method as it is originally published. One should take caution when it is intended to be used in general as it is still a preliminary concept.

In the process of obtaining the added wave resistance of the ship from the in-service data, many uncertainties may be included, such as errors included in the data and estimation of various resistance components. It should be noted that while the Combined method does not include any contribution from steering and yawing to the added resistance, such effects must be expected to be present, to some extent, in the in-service data. However, the following interpretation was obtained in common through the observations of Figs. 32–34. The methods only valid for head waves such as Shopera, Kreitner, and STA2 has the effect of reducing errors in the estimation of the added resistance compared to the case of "no correction". More complicated methods such as CTH and L&P, which reflect hull shape information and can be used in any wave headings, can significantly reduce errors. The Combined method generally has smaller errors than other semi-empirical methods described here and shows noticeable performance in estimating added wave resistance at high wave height, resonance frequency, arbitrary wave headings, and relatively low ship speeds.

5. Conclusions

Estimating the added resistance in arbitrary waves of ships in a proper way has always been a challenging task. In this study, several

Table A.1
Experimental study of added resistance in arbitrary waves for tanker.

Model	L_{pp} [m]	B [m]	F_n [–]	Wave heading [deg].	Reference
VLCC	325	53	0.046/0.073/0.091	180	Lee (2015)
VLCC2	323.6	60	0.058	180	Diao et al. (2019)
S-VLCC	323	60	0.137	0/30/60/90/ 120/150/180	Park et al. (2019a)
SR221C	320	58	0.15	180	Kashiwagi et al. (2004)
KVLCC2	320	58	0/0.05/0.055/0.09/ 0.11/0.142/0.18	0/30/60/90/ 120/150/180	Kashiwagi (1992), Guo and Steen (2011); Sadat-Hosseini et al. (2013); Park et al. (2016); Sprenger et al. (2017); Seo et al. (2021)
Tanker2	310	47.2	0	180	Pinkster (1980)
Aframax	245	44	0.0525	180	Diao et al. (2019)
115k Aframax	239	44	0.156	180	Oh et al. (2015)
ULYSSES	187.3	32.3	0.06/0.12/0.168	120/150/180	Papageorgiou and Ptolemaios (2014); Martinsen (2016)
Handy tanker	176	32.2	0.159/0.171/0.183	180	Chen et al. (2019)
16k Product	145.4	23.4	0.177	180	Li et al. (2016)

Table A.2
Experimental study of added resistance in arbitrary waves for bulk carrier.

Model	L_{pp} [m]	B [m]	F_n [–]	Wave heading [deg].	Reference
JASNAOE-BC	320	58	0.037/0.074/0.124	30/90/150/180	Wicaksono and Kashiwagi (2018); Wicaksono (2019)
Suezmax BC	285	50	0/0.05/0.1/0.15	0/45/90/135/180	Kadomatsu (1988)
JBC	279	45	0.142	180	Kobayashi et al. (2021)
170k BC	279	45	0.128	0/30/60/90/ 120/150/180	Matsumoto (2000)
82k BC	223.5	32.6	0.017	135	Kunpeng et al. (2021)
Panamax BC1	231	38	0.05	180	Diao et al. (2019)
Panamax BC2	216.7	32.3	0.166/0.188	100/120/140/180	Ichinose (2010); Sogihara et al. (2011)
Handymax BC	192	36	0.17	180	Yu et al. (2017)
K-Supramax	192	36	0.172	120/150/180	Lee et al. (2019); Lee et al. (2020)
S-Cb84	178	32.4	0/0.049/0.099/0.166	30/90/150/180	Yasukawa et al. (2019)
S-Cb87	178	32.4	0.142/0.147	180	Yasukawa and Masaru (2020)
Handysize BC	160.4	27.2	0.15	180	Ichinose et al. (2012)
RIOS	2.4	0.4	0.18	180	Iwashita and Kashiwagi (2018)

Table A.3
Experimental study of added resistance in arbitrary waves for liquefied gas carrier.

Model	L_{pp} [m]	B [m]	F_n [–]	Wave heading [deg].	Reference
S-LNGC	290	45	0.13/0.17/0.188	0/30/60/120/150/180	T. Kim et al. (2019), Y. Kim et al. (2019), B.S. Kim et al. (2021)
125k LNG1	273.9	42.3	0.14/0.17/0.2	180	Wichers (1988)
125k LNG2	273	42	0.14/0.17/0.2	90/135/180	Bunnik (1999)
CSSRC LNG	160	26.6	0.036	180	Zheng et al. (2021)

semi-empirical methods were compared using abundant public experimental data with various types, and a new meta-model was proposed combining existing semi-empirical methods. This method is developed for the calculation of added resistance for large fleets of ships, so that robustness, computational efficiency, and applicability to a range of different ship types are priorities.

From the thorough investigation against experimental data, CTH and L&P methods were chosen as a basis for the new model due to high accuracy and the availability against arbitrary wave headings. The two methods have been combined smoothly using a tangent hyperbolic function according to wavelengths and wave headings. The coefficients constituting the combining function were tuned in the direction of minimizing MSE between model experiments and provided for each ship type. The Combined method showed improved results without significantly deviating from the prediction range of existing methods. It has been compared with full-scale measurements of a general cargo and a container ship. For the two vessels, the errors of Kreitner, Shopera, and STA2 were larger with about 14%–45%, and CTH and L&P with 1%–9%, compared to the $RMSE$ of the Combined method. In particular, it was found that the estimation of added resistance in arbitrary waves was more effective in simulating the environment experienced by ships at sea than the methods considering only head seas. It also showed good performance in estimating added wave resistance in the range of high wave height, resonance frequency, arbitrary wave headings, and low ship speed. As can be seen from the comparison of models using experimental test data and full-scale measurements, the Combined method showed good overall performance in various environments. The findings suggest that the new method can be widely applied for any purposes requiring the speed-power performance under the influence of waves such as reference at the initial design stage, speed corrections in sea trials, or overall performance evaluation of a fleet, where detailed hull shape information and advanced tools are not available.

Some of the tank tests in regular waves showed that the interval between wave frequencies was too sparse, that the experiment was not sufficiently conducted in some conditions such as short waves, or that collected samples were scattered even within similar frequency ranges. Due to these problems, it was difficult to estimate added resistance in irregular waves using them. If more experimental data in irregular waves are obtained, detailed comparisons between various estimation methods will be possible, and with more experimental data for various conditions, we expect that the reliability of the model can be improved. Furthermore, since the Combined method is combining two existing methods, it is likely that the Combined method has some of the same

Table A.4
Experimental study of added resistance in arbitrary waves for general cargo ship.

Model	L_{pp} [m]	B [m]	F_n [–]	Wave heading [deg].	Reference
S.A. Van Der Stel	152.5	22.8	0.15/0.2/0.25/0.3	180	Gerritsma and Beukelman (1972); Journee (1976)
VWS 2388 (0/2/3)	146.3	24.4	0.2/0.25	180	Kracht (1984); Lee et al. (2018)
Series 60 (4210)	122.0	16.3	0.2/0.266/0.283	180	Sibul (1971); Ström-Tejsen (1973)
Series 60 (4211)	122.0	16.8	0.237/0.254	180	Ström-Tejsen (1973)
Series 60 (4212)	122.0	17.4	0.1/0.15/0.2/ 0.207/0.222/0.25	10/50/90/ 130/170/180	Ström-Tejsen (1973); Baree et al. (2006)
Series 60 (4213)	122.0	18.1	0.177/0.195	180	Ström-Tejsen (1973)
Series 60 (4214)	122.0	18.8	0.147/0.165	180	Ström-Tejsen (1973)

Table A.5
Experimental study of added resistance in arbitrary waves for container ship.

Model	L_{pp} [m]	B [m]	F_n [–]	Wave heading [deg].	Reference
DTC	355	51	0/0.052/0.139	0/30/60/90/ 120/150/180	Moctar et al. (2012); Yokota et al. (2020); Sprenger et al. (2016, 2017)
WILS II	321	48.4	0.183	180	Söding et al. (2014)
HCNTR	315	48.2	0.204	180	Park et al. (2019b)
CON	300	40	0.2/0.247	0/45/90/ 140/160/180	Tsujimoto et al. (2009, 2012)
Panamax con	270	32.2	0.245	180	Bunnik et al. (2010)
KCS	230	32.2	0.054/0.1/0.16/ 0.26/0.33/0.4	0/45/90/135/180	Simonsen et al. (2013); Sadat-Hosseini et al. (2015); Stocker (2016); Yasukawa et al. (2019); Shivachev et al. (2020)
Feeder	191.1	32.3	0.22	90/120/180	Wada (1991)
S175	175	25.4	0.15/0.2/0.25/ 0.275/0.3	0/30/60/90/ 120/150/180	Fujii (1975); Nakamura and Naito (1977); Yamamoto (1986); Yasukawa (2006); Adnan and Yasukawa (2008)

shortcomings as them, as shown in the analysis of speed effect on wave resistance. If improved versions of the two methods we combined become available, where some of the shortcomings are alleviated, our method should be updated.

CRediT authorship contribution statement

Young-Rong Kim: Conceptualization, Investigation, Methodology, Software, Writing – original draft. **Ehsan Esmailian:** Conceptualization, Software, Writing – review & editing. **Sverre Steen:** Methodology, Writing – review & editing, Supervision.

Declaration of competing interest

The authors declare that they have no known competing financial interests or personal relationships that could have appeared to influence the work reported in this paper.

Data availability

The authors do not have permission to share data.

Acknowledgments

This study is part of the research projects CLIMMS — Climate change mitigation in the maritime sector (Research Council of Norway (RCN) project number 294771).

Appendix A. Experimental dataset

See Tables A.1–A.6

Appendix B. Detailed comparison of semi-empirical methods

Comparison according to the wave heading

As can be seen from the model test results, a peak of head waves was formed near the position where the wavelength and the ship length matched, that is, the radiation force was the largest. As the wave direction went from the head of the ship to the beam, the λ/L of the resonance tended to shorten and the resistance amplitude at the corresponding position tended to decrease.

In Fig. B1(a), the peak position of the STA2 is formed at a shorter λ/L than that of the model test, and this trend also can be seen in other model test cases with a relatively low Froude number on head waves. Since STA2 was mainly developed for the purpose of correction of sea trial results, the evaluation for the low-speed range was perhaps not much considered. According to Holt and Nielsen (2021), a lower Froude number tended to shift the peak value of the transfer function towards λ/L less than 1, which was not in line with the theory. Liu and Papanikolaou (2019) also pointed out that the peak position of STA2 was smaller than the actual value when Froude number was less than 0.15. Moreover, since STA2 was assuming the same response amplitude for 45 degrees off-bow, it did not adequately reflect changes in the resonance frequency position and amplitude of the added resistance according to changes in the encountering angle in head waves (Figs. B1 (a)–(f)).

CTH method adjusts the peak position in arbitrary waves by using an encountered frequency correction factor, and the maximum added resistance is calculated by applying the amplitude adjustment factor and compensation factor for the roll motion. As can be seen from the figure, the peak position and the maximum value of the transfer function gradually decreased as the wave direction moved from bow to stern. On the other hand, the L&P method uses wave heading-based trigonometric functions to approximate the location of resonance frequency and maximum added resistance in various headings. As a result, the peak wavelength position was around $\lambda/L = 1$ at 180 degrees, and as the heading angle decreased, the peak wavelength gradually decreased, and then the peak position was the shortest at 90 degrees. In following waves, the peak position was symmetrically set

Table A.6
Experimental study of added resistance in arbitrary waves for ro-ro/ferry.

Model	L_{pp} [m]	B [m]	F_n [–]	Wave heading [deg].	Reference
Maric cruise	240	32	0.24	180	Liu et al. (2019)
HSVA cruise	220.3	32.2	0.166/0.232	0/30/60/90/ 120/150/18	Ley et al. (2014); Valanto et al. (2015)
PCC	190	32.3	0.249	140/180	Tsujimoto et al. (2009)
RoPax	90	17.8	0/0.087/0.2424	0/180	Sprenger et al. (2015); Liu and Papanikolaou (2020)

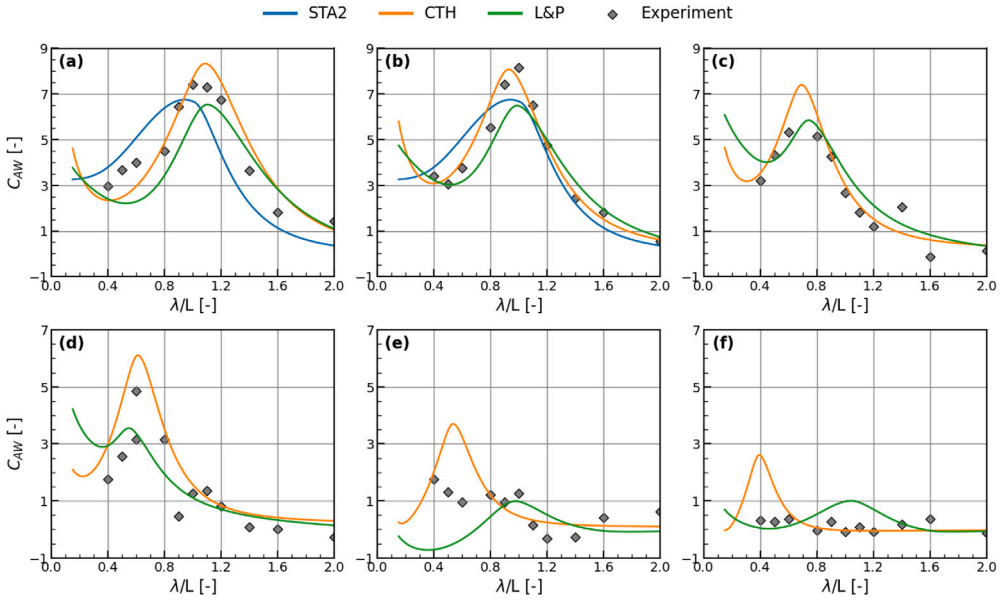

Fig. B1. Added resistance of 170k bulk carrier at $F_n = 0.128$. (a) $\alpha = 180$, (b) $\alpha = 150$, (c) $\alpha = 120$, (d) $\alpha = 90$, (e) $\alpha = 30$, (f) $\alpha = 0$.

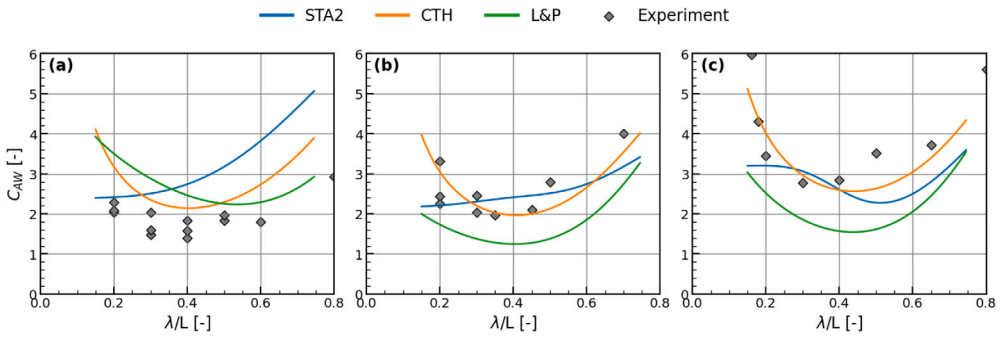

Fig. B2. Added resistance in short waves of (a) SR221C, $F_n = 0.15$, (b) DTC, $F_n = 0.139$, (c) HSVA, $F_n = 0.232$. The figure corresponds to the results of head waves.

based on 90 degrees. In both methods, the maximum added resistance decreased as the wave heading decreased, but as explained earlier, the peak position tended to be somewhat different.

Comparison in short waves

For added resistance in short waves, wave diffraction due to bow reflection dominates, while the effect by wave radiation is almost insignificant. As can be seen from Fig. B2, STA2 has little curvature in the short waves of wavelength less than 0.3. As Yang et al. (2018) pointed out in their paper, since the reflection coefficient of STA2 becomes unity in the short wave region resulting in constant resistance coefficient, STA2 did not properly estimate an increase of added resistance in the corresponding wavelength range in our case studies. On the other hand, L&P and CTH seems to reasonably estimate the tail shape for short waves., The CTH method was most consistent with experimental results in short waves.

Comparison at high Froude number

As illustrated in Fig. B3, STA2 was less accurate in estimating the added wave resistance of a high Froude number than other methods because the maximum resistance at the resonance frequency was underestimated or the positions of the resonance frequency did not match. Meanwhile, in accordance with the bar chart (Fig. 5), the added resistance value estimated from L&P had greater MSE under high-speed operating conditions than that of CTH. As a result of a closer look at the model experiments conducted at Froude number more than 0.25, it generally consisted of datasets of ships that operate in high-speed, such as container ship, general cargo, and Ro-Ro/Ferry. In the case of a container ship at a high Froude number, the two methods provided almost similar results, and even though not described here, there was also no significant difference in the case of other container ships. From such findings, it was determined that this error was not caused by the high Froude number but rather by certain ship types such as general cargo and ro-ro/ferry.

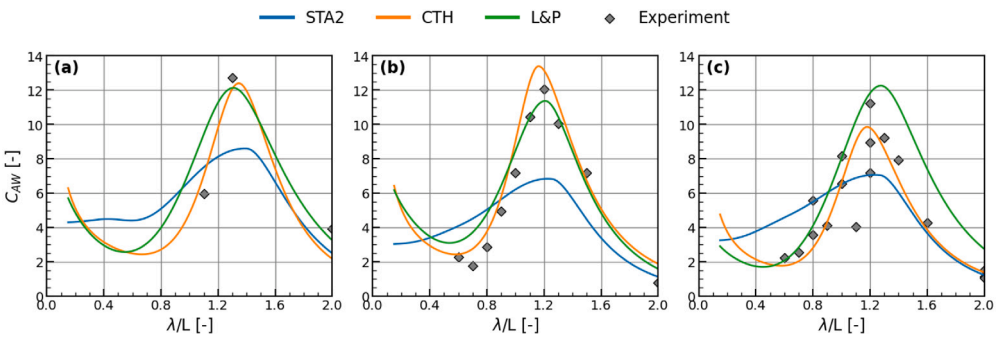

Fig. B3. Added resistance in high Froude number of (a) KCS, F_n = 0.4, (b) S175, F_n = 0.3, (c) S60, F_n = 0.283. The figure corresponds to the results of head waves.

References

Adnan, F., Yasukawa, H., 2008. Experimental investigation of wave-induced motions of an obliquely moving ship. In: Proceedings of 2nd Regional Conference on Vehicle Engineering and Technology.

Auf'm Keller, W., 1973. Extended diagrams for determining the resistance and required power for single-screw ships. Int. Shipbuild. Prog. 20 (225), 133–142.

Baree, M.S., Islam, M.R., Inoue, Y., 2006. An investigation of added resistance of ships in oblique seas. HKIE Trans. 13 (2), 1–8.

Boese, P., 1970. Eine Einfache Methode Zur Berechnung Der Widerstandserhöhung Eines Schiffes Im Seegang. Technical Report.

Boom, H., Huisman, H., Mennen, F., 2013. New guidelines for speed/power trials: Level playing field established for IMO EEDI. SWZ Maritime, Schip En Werf de Zee Foundation, Rotterdam.

Bunnik, T.H., 1999. Seakeeping calculations for ships, taking into account the non-linear steady waves.

Bunnik, T., Van Daalen, E., Kapsenberg, G., Shin, Y., Huijsmans, R., Deng, G., Delhommeau, G., Kashiwagi, M., Beck, B., 2010. A comparative study on state-of-the-art prediction tools for seakeeping. In: Onr Snh 2010, Pasadena, California. Onr, pp. 1–13.

Chen, X., Ren, Y., Xiao, H.-s., Cai, X.-g., Zhu, R.-c., 2019. A MDHOBEM energy radiated method to evaluate added wave resistance of ship. In: The 29th International Ocean and Polar Engineering Conference. OnePetro.

Dalheim, Ø.Ø., Steen, S., 2020. A computationally efficient method for identification of steady state in time series data from ship monitoring. J. Ocean Eng. Sci. 5 (4), 333–345.

Diao, F., Chen, J.-k., Duan, W.-y., Zhou, W.-x., Chen, J., Wei, J.-f., 2019. Prediction of added resistance of a ship in waves at low speed. J. Hydrodyn. 31 (6), 1231–1239.

Faltinsen, O.M., 1980. Prediction of resistance and propulsion of a ship in a seaway. In: Proceedings of the 13th Symposium on Naval Hydrodynamics. Tokyo, 1980.

Fujii, H., 1975. Experimental study on the resistance increase of a ship in regular oblique waves. In: Proc. of 14th ITTC, 1975, Vol. 4. pp. 351–360.

Fujiwara, T., 2006. A new estimation method of wind forces and moments acting on ships on the basis of physical components models. J. Jpn. Soc. Nav. Archit. Ocean Eng. 2, 243–255.

Gerritsma, J., Beukelman, W., 1972. Analysis of the resistance increase in waves of a fast cargo ship. Int. Shipbuild. Prog. 19 (217), 285–293.

Guldhammer, H., Harvald, S.A., 1974. SHIP resistance-effect of form and principal dimensions.(Revised). Danish Technical Press, Danmark, Danmarks Tekniske Hojskole, Kademisk Forlag, St. Kannikestrade 8, DK 1169 Copenhagen.

Guo, B.-j., Steen, S., 2011. Evaluation of added resistance of KVLCC2 in short waves. J. Hydrodynam. Ser. B 23 (6), 709–722.

Guo, B., Steen, S., Deng, G., 2012. Seakeeping prediction of KVLCC2 in head waves with RANS. Appl. Ocean Res. 35, 56–67.

Gupta, P., Taskar, B., Steen, S., Rasheed, A., 2021. Statistical modeling of ship's hydrodynamic performance indicator. Appl. Ocean Res. 111, 102623.

Haiden, T., Janousek, M., Bidlot, J., Buizza, R., Ferranti, L., Prates, F., Vitart, F., 2018. Evaluation of ECMWF Forecasts, Including the 2018 Upgrade. European Centre for Medium Range Weather Forecasts Reading, UK.

Havelock, T.H., 1942. XLVII. The drifting force on a ship among waves. Lond. Edinb. Dub. Philos. Mag. J. Sci. 33 (221), 467–475.

Hollenbach, K.U., 1998. Estimating resistance and propulsion for single-screw and twin-screw ships-ship technology research 45 (1998). Schiffstechnik 45 (2), 72.

Holt, P., Nielsen, U.D., 2021. Preliminary assessment of increased main engine load as a consequence of added wave resistance in the light of minimum propulsion power. Appl. Ocean Res. 108, 102543.

Holtrop, J., 1984. A statistical re-analysis of resistance and propulsion data. Published in International Shipbuilding Progress, ISP, Volume 31, Number 363.

Ichinose, Y., 2010. Estimation of added resistance in waves in a ballast condition. J. Jpn. Soc. Nav. Archit. Ocean Eng. 11, 109–116.

Ichinose, Y., Tsujimoto, M., Shiraishi, K., Sogihara, N., 2012. Decrease of ship speed in actual seas of a bulk carrier in full load and ballast conditions-model test and onboard measurement. J. Jpn. Soc. Nav. Archit. Ocean Eng. 15, 37–45.

IMO, 2016. Supplementary information on the draft revised guidelines for determining minimum propulsion power to maintain the manoeuvrability of ships in adverse conditions, submitted by Denmark, Germany and Japan. MEPC70/INF.30.

ITTC, 2005. Recommended procedures and guidelines: Full scale measurements speed and power trials analysis of speed.

ITTC, 2017. Recommended procedures and guidelines: Preparation, conduct and analysis of speed/power trials.

Iwashita, H., Kashiwagi, M., 2018. An innovative EFD for studying ship seakeeping. In: Proceedings of 33rd IWWWFB (Guidel-Plages, France). pp. 85–88.

Jinkine, V., Ferdinande, V., 1974. A method for predicting the added resistance of fast cargo ships in head waves. Int. Shipbuild. Prog. 21 (238), 149–167.

Joncquez, S., 2009. Second-Order Forces and Moments Acting on Ships in Waves (Ph. D. Thesis). Technical University of Denmark, Copenhagen, Denmark.

Joosen, W., 1966. Added resistance of ships in waves. In: Proc. 6th Symp. on Naval Hydrodynamics. Washington, pp. 637–647.

Journee, J.M., 1976. Motions, Resistance and Propulsion of a Ship in Longitudinal Regular Waves. TUDelft, Faculty of Marine Technology, Ship Hydromechanics Laboratory, Report No. 428.

Kadomatsu, K., 1988. Study on the Required Minimum Output of Main Propulsion Engine Considering Maneuverability in Rough Sea. Yokohama National University.

Kashiwagi, M., 1992. Added resistance, wave-induced steady sway force and yaw moment on an advancing ship.

Kashiwagi, M., Sugimoto, K., Ueda, T., Yamasaki, K., Arihama, K., Kimura, K., Yamashita, R., Itoh, A., Mizokami, S., 2004. An analysis system for propulsive performance in waves. J.-Kansai Soc. Nav. Archit. Jpn. 67–82.

Kim, K.-H., Kim, Y., 2011. Numerical study on added resistance of ships by using a time-domain rankine panel method. Ocean Eng. 38 (13), 1357–1367.

Kim, B.-S., Oh, M.-J., Lee, J.-H., Kim, Y.-h., Roh, M.-I., 2021. Study on hull optimization process considering operational efficiency in waves. Processes 9 (5), 898.

Kim, Y., Park, D.-M., Lee, J.-H., Lee, J., Kim, B.-S., Yang, K.-K., Oh, S., Lee, D.-Y., 2019. Numerical analysis and experimental validation of added resistance on ship in waves. J. Ship Res. 63 (04), 268–282.

Kim, T., Yoo, S., Kim, H.J., 2021. Estimation of added resistance of an LNG carrier in oblique waves. Ocean Eng. 231, 109068.

Kim, T., Yoo, S., Oh, S., Kim, H.J., Lee, D., Kim, B., 2019. Numerical and experimental study on the estimation of added resistance of an LNG carrier in waves. Int. J. Offshore Polar Eng. 29 (01), 24–32.

Kitamura, F., Ueno, M., Fujiwara, T., Sogihara, N., 2017. Estimation of above water structural parameters and wind loads on ships. Ships Offshore Struct. 12 (8), 1100–1108.

Kobayashi, H., Kume, K., Orihara, H., Ikebuchi, T., Aoki, I., Yoshida, R., Yoshida, H., Ryu, T., Arai, Y., Katagiri, K., et al., 2021. Parametric study of added resistance and ship motion in head waves through RANS: Calculation guideline. Appl. Ocean Res. 110, 102573.

Kracht, A., 1984. Einfluss Des Bugwulstes Auf Den Leistungsbedarf Eines Schiffes Im Seegang. Forschungszentrum des Dt. Schiffbaus.

Kreitner, J., 1939. Heave, pitch and resistance of ships in a seaway. Trans. Royal Inst. Nav. Archit.,'London 87.

Kunpeng, C., Fan, Y., Yunlong, D., 2021. RANS CFD seakeeping simulation for an 82k DWT vessel in head and oblique waves. In: J. Phys.: Conf. Ser.. 1834, (1), IOP Publishing, 012009.

Kuroda, M., Tsujimoto, M., Fujiwara, T., Ohmatsu, S., Takagi, K., 2008. Investigation on components of added resistance in short waves. J. Jpn. Soc. Nav. Archit. Ocean Eng. 8, 171–176.

Lang, X., Mao, W., 2020. A semi-empirical model for ship speed loss prediction at head sea and its validation by full-scale measurements. Ocean Eng. 209, 107494.

Lang, X., Mao, W., 2021. A practical speed loss prediction model at arbitrary wave heading for ship voyage optimization. J. Mar. Sci. Appl. 20 (3), 410–425.

Lee, S.-M., 2015. Experimental study on added resistance of VLCC for ship's operating condition in waves. J. Korean Soc. Mar. Environ. Saf. 21 (3), 240–245.
Lee, J.-H., Kim, Y., Kim, B.-S., Gerhardt, F., 2021. Comparative study on analysis methods for added resistance of four ships in head and oblique waves. Ocean Eng. 236, 109552.
Lee, J.-H., Kim, B.-S., Kim, B.-S., Lee, J., Kim, Y., Paik, K.-J., Kim, T., Yang, J.-H., Song, K.-H., Kim, P., et al., 2020. Comparative study on added resistance of a bulk carrier in regular head and oblique waves. In: The 30th International Ocean and Polar Engineering Conference. OnePetro.
Lee, J.-h., Kim, S.-s., Lee, S.-s., Kang, D., Lee, J.-c., 2018. Prediction of added resistance using genetic programming. Ocean Eng. 153, 104–111.
Lee, C.-M., Yu, J.-W., Choi, J.-E., Lee, I., 2019. Effect of bow hull forms on the resistance performance in calm water and waves for 66k DWT bulk carrier. Int. J. Nav. Archit. Ocean Eng. 11 (2), 723–735.
Ley, J., Sigmund, S., el Moctar, O., 2014. Numerical prediction of the added resistance of ships in waves. In: International Conference on Offshore Mechanics and Arctic Engineering, Vol. 45400. American Society of Mechanical Engineers, V002T08A069.
Li, C., Ma, X., Chen, W., Li, J., Dong, G., 2016. Experimental investigation of self propulsion factor for a ship in regular waves. Shipbuild China 57 (1), 1–8.
Liu, S., 2020. Revisiting the influence of a ship's draft on the drift force due to diffraction effect. Ship Technol. Res. 67 (3), 175–180.
Liu, S., Papanikolaou, A., 2016. Fast approach to the estimation of the added resistance of ships in head waves. Ocean Eng. 112, 211–225.
Liu, S., Papanikolaou, A., 2019. Approximation of the added resistance of ships with small draft or in ballast condition by empirical formula. Proc. Inst. Mech. Eng. M 233 (1), 27–40.
Liu, S., Papanikolaou, A., 2020. Regression analysis of experimental data for added resistance in waves of arbitrary heading and development of a semi-empirical formula. Ocean Eng. 206, 107357.
Liu, S., Papanikolaou, A., Feng, P., Fan, S., 2019. A multi-level approach to the prediction of the added resistance and powering of ships in waves. In: International Conference on Offshore Mechanics and Arctic Engineering, Vol. 58851. American Society of Mechanical Engineers, V07BT06A037.
Liu, S., Shang, B., Papanikolaou, A., Bolbot, V., 2016. Improved formula for estimating added resistance of ships in engineering applications. J. Mar. Sci. Appl. 15 (4), 442–451.
Martinsen, M., 2016. A Design Tool for Estimating Wave Added Resistance of Container Ships (Master's Thesis). Technical University of Denmark, Copenhagen, Denmark.
Maruo, H., 1957. The excess resistance of a ship in rough seas. Int. Shipbuild. Prog. 4 (35), 337–345.
Maruo, H., 1960. Wave resistance of a ship in regular head seas. Bull. Fac. Eng. Yokohama Natl. Univ. 9, 73–91.
Maruo, H., 1963. Resistance in waves, research on seakeeping qualities of ships in Japan. Soc. Nav. Archit. Jpn. 8, 67–102.
Matsumoto, K., 2000. Development of energy saving bow shape at sea. In: Proc. of the 4th Osaka Colloquium on Seakeeping Performance of Ships, 2000. pp. 479–485.
Minsaas, K., 1982. Grunnlag for Fartsprognoser. Technical Report, Marintek (former: Norges Hydrodynamiske Laboratorier.
Moctar, O.e., Shigunov, V., Zorn, T., 2012. Duisburg test case: Post-panamax container ship for benchmarking. Ship Technol. Res. 59 (3), 50–64.
Mourkogiannis, D., Liu, S., 2021. Investigation of the influence of the main dimensional ratios of a ship on the added resistance and drift force in short waves. In: The 31st International Ocean and Polar Engineering Conference. OnePetro.
Nakamura, S., Naito, S., 1977. Propulsive performance of a container ship in waves. J. Soc. Nav. Archit. Jpn. 15.
Oh, S., Yang, J., Park, S.-H., 2015. Computational and experimental studies on added resistance of aframax-class tankers in head seas. J. Soc. Nav. Archit. Korea 52 (6), 471–477.
Orihara, H., Miyata, H., 2003. Evaluation of added resistance in regular incident waves by computational fluid dynamics motion simulation using an overlapping grid system. J. Mar. Sci. Technol. 8 (2), 47–60.
Papageorgiou, S., Ptolemaios, I., 2014. A comparison of methods for predicting the wave added resistance of slow steaming ships.
Papanikolaou, A., Zaraphonitis, G., Bitner-Gregersen, E., Shigunov, V., El Moctar, O., Soares, C.G., Reddy, D.N., Sprenger, F., 2015. Energy efficient safe ship operation (SHOPERA). In: SNAME 5th World Maritime Technology Conference. OnePetro.
Park, D.-M., Kim, Y., Seo, M.-G., Lee, J., 2016. Study on added resistance of a tanker in head waves at different drafts. Ocean Eng. 111, 569–581.
Park, D.-M., Lee, J.-H., Jung, Y.-W., Lee, J., Kim, Y., Gerhardt, F., 2019a. Experimental and numerical studies on added resistance of ship in oblique sea conditions. Ocean Eng. 186, 106070.
Park, D.-M., Lee, J.-H., Lee, J., Kim, B.-S., Kim, B.-S., Yang, K.-K., Kim, Y., Lee, Y.-G., Kim, T., Yang, J.-H., et al., 2019b. Comparative study on added resistance of a container ship in waves. In: The 29th International Ocean and Polar Engineering Conference. OnePetro.
Pinkster, J.A., 1980. Low frequency second order wave exciting forces on floating structures.
Sadat-Hosseini, H., Toxopeus, S., Kim, D.H., Castiglione, T., Sanada, Y., Stocker, M., Simonsen, C., Otzen, J.F., Toda, Y., Stern, F., 2015. Experiments and computations for KCS added resistance for variable heading. In: SNAME 5th World Maritime Technology Conference. OnePetro.
Sadat-Hosseini, H., Wu, P.-C., Carrica, P.M., Kim, H., Toda, Y., Stern, F., 2013. CFD verification and validation of added resistance and motions of KVLCC2 with fixed and free surge in short and long head waves. Ocean Eng. 59, 240–273.
Salvesen, N., 1978. Added resistance of ships in waves. J. Hydronaut. 12 (1), 24–34.
Seo, M.G., Ha, Y.J., Nam, B.W., Kim, Y., 2021. Experimental and numerical analysis of wave drift force on KVLCC2 moving in oblique waves. J. Mar. Sci. Eng. 9 (2), 136.
Seo, M.-G., Park, D.-M., Yang, K.-K., Kim, Y., 2013. Comparative study on computation of ship added resistance in waves. Ocean Eng. 73, 1–15.
Shaher Sabit, A., 1972. An analysis of the series 60 results. Int. Shipbuild. Prog. 19 (211), 81–97.
Shigunov, V., El Moctar, O., Papanikolaou, A., Potthoff, R., Liu, S., 2018. International benchmark study on numerical simulation methods for prediction of manoeuvrability of ships in waves. Ocean Eng. 165, 365–385.
Ships, I., 2015. Marine technology—Guidelines for the assessment of speed and power performance by analysis of speed trial data. ISO: Geneva, Switzerland.
Shivachev, E., Khorasanchi, M., Day, S., Turan, O., 2020. Impact of trim on added resistance of KRISO container ship (KCS) in head waves: An experimental and numerical study. Ocean Eng. 211, 107594.
Sibul, O., 1971. Measurements and Calculations of Ship Resistance in Waves. Technical Report, California Univ Berkeley Coll of Engineering.
Sigmund, S., El Moctar, O., 2018. Numerical and experimental investigation of added resistance of different ship types in short and long waves. Ocean Eng. 147, 51–67.
Simonsen, C.D., Otzen, J.F., Joncquez, S., Stern, F., 2013. EFD and CFD for KCS heaving and pitching in regular head waves. J. Mar. Sci. Technol. 18 (4), 435–459.
Simonsen, C., Otzen, J., Nielsen, C., Stern, F., 2014. CFD prediction of added resistance of the KCS in regular head and oblique waves. In: 30th Symposium on Naval Hydrodynamics. pp. 2–7.
Söding, H., Shigunov, V., Schellin, T.E., Moctar, O.e., 2014. A rankine panel method for added resistance of ships in waves. J. Offshore Mech. Arct. Eng. 136 (3).
Sogihara, N., Tsujimoto, M., Ichinose, Y., Minami, Y., Sasaki, N., Ken, T., 2011. Performance prediction of a blunt ship in oblique waves. J. Jpn. Soc. Nav. Archit. Ocean Eng. 12, 9–15.
Sprenger, F., Hassani, V., Maron, A., Delefortrie, G., Van Zwijnsvoorde, T., Cura-Hochbaum, A., Lengwinat, A., 2016. Establishment of a validation and benchmark database for the assessment of ship operation in adverse conditions. In: International Conference on Offshore Mechanics and Arctic Engineering, Vol. 49927. American Society of Mechanical Engineers, V001T01A039.
Sprenger, F., Maron, A., Delefortrie, G., Hochbaum, A., Fathi, D., 2015. Mid-term review of tank test results. SHOPERA Project Deliverable D, 3.
Sprenger, F., Maron, A., Delefortrie, G., Van Zwijnsvoorde, T., Cura-Hochbaum, A., Lengwinat, A., Papanikolaou, A., 2017. Experimental studies on seakeeping and maneuverability of ships in adverse weather conditions. J. Ship Res. 61 (03), 131–152.
Steen, S., Aarsnes, J.V., 2014. Experimental methods in marine hydrodynamics. In: Lecture Notes.
Stocker, M.R., 2016. Surge Free Added Resistance Tests in Oblique Wave Headings for the KRISO Container Ship Model. The University of Iowa.
Ström-Tejsen, J., 1973. Added resistance in waves. In: Paper 3 of the Annual Meeting New York of the Society of Naval Architects and Marine Engineers, SNAME Transactions 1973, Paper: T1973-1 Transactions. Naval Ship Research and Development Center, Bethesda, Maryland, USA, Research and Development Report, Ship Performance Department.
Takahashi, T., 1988. A practical prediction method of added resistance of a ship in waves and the direction of its application to hull form design. Trans. West-Jpn. Soc. Nav. Archit. 75, 75–95.
Tsujimoto, M., Kuroda, M., Shibata, K., Sogihara, N., Takagi, K., 2009. On a calculation of decrease of ship speed in actual seas. J. Jpn. Soc. Nav. Archit. Ocean Eng. 9, 79–85.
Tsujimoto, M., Kuroda, M., Shiraishi, K., Ichinose, Y., Sogihara, N., 2012. Verification on the resistance test in waves using the actual sea model basin. J. Jpn. Soc. Nav. Archit. Ocean Eng. 16, 33–39.
Tsujimoto, M., Shibata, K., Kuroda, M., Takagi, K., 2008. A practical correction method for added resistance in waves. J. Jpn. Soc. Nav. Archit. Ocean Eng. 8, 177–184.
Ursell, F., 1947. The effect of a fixed vertical barrier on surface waves in deep water. In: Mathematical Proceedings of the Cambridge Philosophical Society, Vol. 43, no. 3. Cambridge University Press, pp. 374–382.
Valanto, P., Hong, Y., et al., 2015. Experimental investigation on ship wave added resistance in regular head, oblique, beam, and following waves. In: The Twenty-Fifth International Ocean and Polar Engineering Conference. International Society of Offshore and Polar Engineers.
Wada, Y., 1991. A study on speed drop of a ship in oblique waves. In: Transactions of the West-Japan Society of Naval Architects. The Japan Society of Naval Architects and Ocean Engineers, pp. 113–128.
Wang, J., Bielicki, S., Kluwe, F., Orihara, H., Xin, G., Kume, K., Oh, S., Liu, S., Feng, P., 2021. Validation study on a new semi-empirical method for the prediction of added resistance in waves of arbitrary heading in analyzing ship speed trial results. Ocean Eng. 240, 109959.
Wicaksono, A., 2019. A unified computation method for seakeeping-maneuvering of a ship in waves using slender-ship theory and MMG model.

Wicaksono, A., Kashiwagi, M., 2018. Wave-induced steady forces and yaw moment of a ship advancing in oblique waves. J. Mar. Sci. Technol. 23 (4), 767–781.
Wichers, J.E.W., 1988. A simulation model for a single point moored tanker.
Yamamoto, O., 1986. Study on an approximate calculation method of resistance increase in oblique regular waves. J. Kansai Soc. Nav. Archit. (201).
Yang, K.-K., Kim, Y., Jung, Y.-W., 2018. Enhancement of asymptotic formula for added resistance of ships in short waves. Ocean Eng. 148, 211–222.
Yasukawa, H., 2006. Simulations of ship maneuvering in waves (1 st report: Turning motion). J. Jpn Soc. Nav. Archit. Ocean Eng. 4, 127–136.
Yasukawa, H., Hirata, N., Matsumoto, A., Kuroiwa, R., Mizokami, S., 2019. Evaluations of wave-induced steady forces and turning motion of a full hull ship in waves. J. Mar. Sci. Technol. 24 (1), 1–15.
Yasukawa, H., Masaru, T., 2020. Impact of bow shape on added resistance of a full hull ship in head waves. Ship Technol. Res. 67 (3), 136–147.
Yokota, S., Kuroda, M., Fukasawa, R., Ohba, H., Tsujimoto, M., 2020. Detailed study on the behavior of ships in very short waves. In: International Conference on Offshore Mechanics and Arctic Engineering, Vol. 84386. American Society of Mechanical Engineers, V06BT06A020.
Yu, J.-W., Lee, C.-M., Lee, I., Choi, J.-E., 2017. Bow hull-form optimization in waves of a 66,000 DWT bulk carrier. Int. J. Nav. Archit. Ocean Eng. 9 (5), 499–508.
Zheng, M., Ni, Y., Wu, C., Jo, H., 2021. Experimental investigation on effect of sloshing on ship added resistance in head waves. Ocean Eng. 235, 109362.